Fall 2019

Development of Multicomponent EAM Potential for Ni-Based Superalloy

Muztoba Rabbani
Missouri State University, Muztoba333@live.missouristate.edu

DEVELOPMENT OF MULTICOMPONENET EAM POTENTIAL FOR NI-BASED SUPERALLOY

A Master's Thesis

Presented to

The Graduate College of

Missouri State University

In Partial Fulfillment

Of the Requirements for the Degree

Master of Science, Material Science

By

Muztoba Rabbani

December 2019

DEVELOPMENT OF MULTICOMPONENET EAM POTENTIAL FOR NI-BASED SUPERALLOY

Physics, Astronomy, and Material Science

Missouri State University, December 2019

Master of Science

Muztoba Rabbani

ABSTRACT

We initiated the development of multi-component EAM potentials for Aluminides and Carbides, key phases in Ni-based Superalloys. The goal is to utilize the MD simulation to understand the deformation dynamics that contribute to the formation of voids and creep initiation. For this purpose, we constructed the raw data from ab-initio (molecular dynamics) MD simulations fed into the potential development code and used Nickel as the base metal with the addition of a number of various elements including Aluminum, Chromium, Tungsten. We then developed the EAM potentials for the aluminide and carbide phases using the force-fitting code MEAMfit. Our generated potential reproduces the fundamental properties of the Ni_3Al and $Mo_{23}C_6$ phases. We verified further the EAM potential through the thermal stability test at different temperatures and by reproducing the elastic constants consistent with the experimental values.

KEYWORDS: interatomic potential, molecular dynamics, ab-initio data, Ni3Al, Thermal Stability, elastic constants.

DEVELOPMENT OF MULTICOMPONENET EAM POTENTIAL FOR NI-BASED SUPERALLOY

By

Muztoba Rabbani

A Master's Thesis
Submitted to the Graduate College
Of Missouri State University
In Partial Fulfillment of the Requirements
For the Degree of Master of Science, Material Science

December 2019

Approved:

Ridwan Sakidja, Ph.D., Thesis Committee Chair

Kartik Ghosh, Ph.D., Thesis Committee Member

Tiglet Besara, , Ph.D., Thesis Committee Member

Julie Masterson, Ph.D., Dean of the Graduate College

ACKNOWLEDGEMENTS

I am very much thankful to my supervisor Dr. Ridwan Sakidja for guidance and constant support through this 2 years of Masters life. I will always be greatful to him for providing this research opportunity and also for mentoring me in everystep.

I am also thankful to Dr. Kartik Ghosh for just not being my teacher but also for been there as a guardian for us. We learned a lot from him. And I am thankful to our Departmental Head Dr. Robert Mayanovic and thankful to Dr. Tiglet Bisara for serving as my thesis committee.

I am also thankful to my colleagues, Nirmal Baishnab, Sabila Kader Pinky, Rajan Khadka and Tyler McGilvry James. They helped me a lot in this research work.

I dedicate this thesis to my Golam Rabbani (father), Anzuman Ara (mother), Murtoza Rabbani (brother).

TABLE OF CONTENTS

LIST OF TABLES

LIST OF FIGURES

INTRODUCTION

History of Ni-Based Superalloy

Ni-based Superalloy has been used for aircraft turbine engines for years. Aircraft turbine engines are a very complicated machine as it needs to meet some specific criteria for being suitable for its work environment. And those crucial requirements are being in the high temperature and high-pressure situation.

High pressured parts of the turbine engine causes for high temperature and that part is also the highest stress part of the body. Especially the rim part is the challenging part as it reaches 760°C to 815°C[1]. And to confront those issues specialized Ni-based superalloy was needed. Apart from temperature issues alloys are affected by many commercial effects. Low-component cost, life-cycle costs, fuel efficiency, and emissions are also crucial facts that compromise between performance and economics [1]. With the rising requirements of turbine engines material has been developed accordingly to meet all these criteria.

Formation of Ni-based Superalloy

Ni-based Superalloy is mainly composed of Cr, Co, Mo, W, Al, Ti, Ta [2]. Properties of these allowing elements are well studied [3]. Cr helps in hot corrosion resistance as it causes the formation of a protective Cr2O3 oxide scale. Cr, Co & Mo gave the are the solid solution strengthening elements Cr_2O_3. These alloys have Ni_3Al based γ' phase particle which are in high volume fractional strengthen order. Al also has vital role in the formation of stable Al_2O_3. Figure 1, is the microscopic photo of Ni-based SuperAlloy.

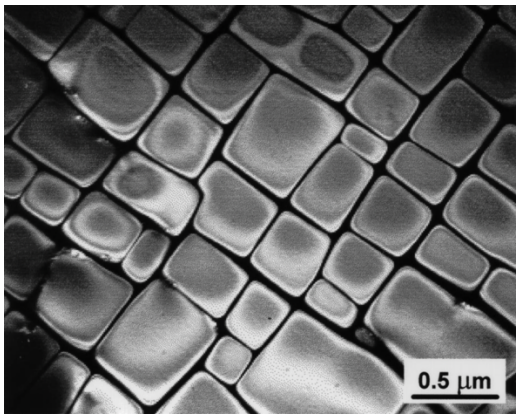

Figure 1. First Generation $\gamma - \gamma'$ Ni-based SuperAlloy

The single crystal SuperAlloy did not have voluntary trivial elements such as C, B, Hf, Zr which are generally being used for grain boundaries. These results in the increase of incipient melting temperature from 1240 ºC to 1330 ºC.

Different alloy composition was introduced by engines manufacturers to improve the creep strength. Mechanical properties were also improved by balancing the various alloy's elements.

The second-generation single-crystal SuperAlloy came with the addition of rhenium instead of other stubborn elements such as W. 3 wt.% of rhenium was added to the alloy to the single crystal nickel-based superalloys which improved the temperature capability by 30ºC [4]. The rhenium bearing alloy formed topological close-packed brittle phases as σ, μ or P phases during high temperature presences and these hampered the stability. These topological close-packed phases induce deleterious effects on mechanical properties like ductility loss, impacts strength decrease and creep strength decrease[5].

And also, to γ matrix is partitioned preferentially by rhenium. Re replaced and carefully balanced the other former elements Mo, Co and W to avoid supersaturation [2] and that causes Re-rich topological close-packed phase particles. The Cr percentage from first-generation single

crystal alloy decreases from 8 wt.% to 5-7 wt.% in the second generation. But this amount is enough to ensure corrosion resistance and give optimized creep strength.

For keeping the environmental properties in priority Mo was kept low level because this element has a negative effect on corrosion resistance of the Ni-based SuperAlloy. But rhenium has a positive influence on oxidation resistance and hot corrosion. But the excessive addition of rhenium caused some problems like freckles that were observed in single crystal superalloys. Another drawback is for the rotating parts of the aeronautical engines caused by the increase density of rhenium.

For improving the high-temperature endurance designer incorporated more rhenium into the alloy and that becomes about 6 wt.%. The reason was to get better creep strength avoiding the density issue and also avoiding the precipitation of topologically close-packed phases. CMSX-10 developed by Cannon-Muske [6] is one of them. In the third generation because the instability was still a problem because it was tough to get the right balance of the allowing elements. And these lead to the precipitation of topologically close-packed phases. Cr was decreased to 2 to 4.2 wt.% for keeping the alloys away from topological close-packed phases. An important difference in the third-generation designs was including C and V to Rene′ N6 [7] in order to increase the castability and low angle tolerance grain boundaries. Yttrium was also incorporated in Rene′ N6 to enhance the adherence on the protective layer of Al_2O_3 at high temperature and Hf was used in single crystal superalloys to improve coatability. But at the same time because of the low Cr third generation superalloys became vulnerable to hot corrosion resistance.

Third generation single crystal alloys show better stress rupture strength than second-generation alloy Rene′ N5. Rene′ N6 was improved by 30º C from Rene′ N5[7]. The creep

strength of CMSX[10] was benefited at 982ºC from CMSX-4 but decreases with increasing exposure times[8]. This tells the third generation is not always better than the second generation. But third-generation single-crystal maintains high creep resistance at above 1100ºC. And also the tensile strength of the third generation is better than the first and second generation with the highest strength at 760ºC maintaining a good ductility[8].

Micro-Constitution of Superalloy

Face-centered cubic (FCC) nickel is the main element of the superalloy and five to ten more elements contain the 40 wt.%. The nickel-aluminum is the binary basis of the superalloy. When aluminum is added to γ phase of the nickel a second phase is formed. This phase has a combination of Ni_3Al and is known as γ'phase. And it has the structure of $L1_2$ crystal[9]. The high volume fraction of γ' phase makes the superalloy stronger. These γ and γ' phases are the main constituents of superalloy microstructure. Where W, Nb, Re contributes to the strengthening to γ phase there Ti, Ta and Nb improves the strengthening for γ' phase[10]. Cr, Y, La contribute to oxidation and corrosion. Figure 2 shows the allowing elements in superalloy.

IIA	IIIA	IVB						
	B 0.097	C 0.077						
	Al 0.143							
		Ti 0.147	V 0.132	Cr 0.125		Fe 0.124	Co 0.125	Ni 0.125

	Y 0.181	Zr 0.158	Nb 0.143	Mo 0.136		Ru 0.134		
		Hf 0.159	Ta 0.147	W 0.137	Re 0.138			

$\gamma' former$ Minor Additionγ former

Figure 2. Alloying elements present in Ni-based SuperAlloy adapted from reference [3].

Properties of Superalloy

In this section Properties of Nickel-based SuperAlloy will be discussed. A great portion of the turbine engine is made of SuperAlloy because of the unique physical and mechanical properties. Creep, deformation, tensile and cycling crack are the main concern in the mechanical properties. Depending on the microstructure of the superalloy above-mentioned properties vary from one alloy to another.

Tensile Properties. The typical tensile strength of Ni-based superalloy is 1200-1600MPa at room temperature and the yield strength range is 900-1300MPa[11][12]. Turbine disks are designed to have higher strength below 1073K to protect the disk in the engines overspeeding events. This tensile property remains the same unless the temperature exceeds 1123K. Another interesting thing is two-phase superalloy is stronger than any single-phase bulk form [13].

This two-phase strengthing comes from multiple sources like microstructural sources, solid solution strengthening, the interaction of dislocation with precipitates, grain size strengthening. Maximizing the tensile strength is a major challenge

Creep Properties. Superalloys remain under pressure at high temperature for a long

the time that makes it vulnerable to creep deformation. Resistance to this creep deformation becomes essential. This property might vary from one alloy to another as cast blade alloy will be under 1100ºC and disk alloy will be under 700ºC only. Two-phase alloys generally have much more creep resistance than single-phase alloys[9]. Creep rupture is highly dependent on the microstructural property. Creep rate is controlled by the diffusion coefficient, low interdiffusion causes high creep rupture. Also, elements like Re, W, and Mo are beneficial in creep-resistance. With advances in the processing maximum temperature of the creep rupture also increased. Below 800ºC temperature creep deformation is very unlikely in Superalloy. Dislocation in superalloy takes place generally in <110> {111} slip system. The size of γ', volume fraction and alloy composition influence these shearing processes.

But at an intermediate temperature, the deformation is confined to γ matrix rather than in γ'. Many of the measurements are not easy to calculate experimentally when high temperature and liquid phase is involved [14]. And many properties of alloys are complicated to study because of the lower symmetry and long-range strains around defects. Another argued topic is the forming of a cluster because of the Re. Experimental study on Re with field ion microscopy and atom probe study showed Rhenium forms cluster. With Atomic probe field ion microscopy (AP-FIM) measurements it was shown that Re dissolves in matrix phase and clusters together in a group[14]. Re holds back the coarsening and dislocation motion in γ' phase and thus it improved many mechanical properties in Superalloy. But in another experimental research on Ni-Re alloy showed that Re does not form clusters. Mottura [15] in an experiment with local electrode atom probe, x-ray absorption technique and atom probe tomography showed in γ phase and Ni-Al binary alloy Re does not have any effect in forming clusters.

Ab initio Simulations

History. After the 20th century, the atomic structure of matter was discovered which later leads to many quantum mechanical formulation laws. With the existence of electron and nuclei into the account precise prediction of many physical phenomena was being calculated. After the discovery of the electron in the 1890s quantum theories started to develop. Though the Bohr model has fundamental flaws it inspired many physicists led to quantum mechanical theories. A big milestone change came to these theories with the introduction of wave-particle duality. Though this concept was already in the field from 1905 for photons and lightwave from 1924 it was generalized for all particles. It says

$$\lambda = \frac{h}{p} \tag{1.1}$$

Here λ is the wavelength of a particle, p is the momentum and h is the Planck's constant. Based on this theory particle-wave concept was established. Schrodinger found the equation of the propagation of the wave which later helped to get the mathematical description of the quantum system. The generalized version of quantum theory that we know today is given by Dirac. Dirac introduced Bra-Ket notation which represents the wave functions or quantum states with vectors.

The Quantum Many-Body Problem. In quantum mechanics, the Hamiltonian operator for a system of electrons and nuclei is written as

$$\hat{H} = \hat{H}_{NN} + \hat{H}_{ee} + \hat{H}_{Ne} \tag{1.2}$$

Here $\hat{H}_{NN}$ is the Hamiltonian energy for nuclei and $\hat{H}_{ee}$ is the energy for electrons and $\hat{H}_{Ne}$ is the interaction between nuclei and electron.

$$\widehat{H}_{NN} = -\sum_{\alpha} \frac{\hbar}{2M_{\alpha}} \nabla_{\alpha}^2 + \frac{1}{2} \sum_{\substack{\alpha,\beta \\ \alpha \neq \beta}} \frac{Z_{\alpha} Z_{\beta} e^2}{|R_{\alpha} - R_{\beta}|} \tag{1.3}$$

Here upper case indicates nuclei and lower case the electrons. $\widehat{H}_{ee}$ is equivalent to $\widehat{H}_{NN}$ but for the electrons=

$$\widehat{H}_{ee} = -\sum_{i} \frac{\hbar^2}{2m} \nabla_i^2 + \sum_{\substack{i,j \\ i \neq j}} \frac{e^2}{|r_i - r_j|} \tag{1.4}$$

And the last term of electron nuclei interaction

$$\widehat{H}_{Ne} = -\sum_{\alpha} \sum_{i} \frac{Z_{\alpha} e^2}{|r_i - R_{\alpha}|} \tag{1.5}$$

The ground state energy of the quantum system can be calculated with the time-independent Schrodinger equation,

$$\widehat{H} \Psi(r_i, R_{\alpha}) = E \, \Psi(r_i, R_{\alpha}), \tag{1.6}$$

and the many-body wavefunction

$$\psi(r_i, R_{\alpha}) \equiv \psi(r_1, \ldots., r_n, R_1, \ldots., R_N) \tag{1.7}$$

This depends on the co-ordinates of electrons and nuclei.

Now comes the tough part. The Hamiltonian Eq. (1.1) is not possible to calculate. Even with the small system with few atoms, the problem becomes so complex that is goes beyond the capability of the currently available computer. For example, a single oxygen atom with eight electrons the atoms this data becomes extremely huge. If in a many-body wavefunction for storing a single value 10 bytes are needed and the storage capacity for the entire function for $10 \times 10 \times 10$ grid, will be a trillion 1TB hard drives.

That's why physicists came up with some approximation to solve many-body problems.

The Born-Oppenheimer Approximation

The Born-Oppenheimer approximation is also known as an adiabatic approximation and this is the very fundamental part of theoretical approaches to quantum mechanics. We know the mass of the electrons is much smaller than the mass of the nuclei and in the Born-Oppenheimer Approximation the kinetic energy of the nuclei is considered to be small comparing to the electron. This approximation is different in many ways

- Nuclei are decoupling from electrons
- Electronic wavefunctions follow the positions of the nuclear not the speed of it
- No exchange of energy between the electrons and nuclei

Based on this assumption the first term of (1.2) can be neglected and the Schrodinger equation can be written as,

$$\left[\widehat{H}_{ee} + \widehat{H}_{Ne} + \frac{1}{2}\sum_{\alpha,\beta}\frac{Z_\alpha Z_\beta e^2}{|R_\alpha - R_\beta|}\right]\phi = \varepsilon\phi. \tag{1.8}$$

The energy ϵ and the wavefunction ϕ depends on nuclear position

$$\phi = \phi(r_i, \{R_\alpha\}) and\ \varepsilon = \varepsilon(\{R_\alpha\}) \tag{1.9}$$

Ignoring the kinetic energy for the nuclei, the Hamiltonian can be written as,

$$\widehat{H} = \hat{T} + \hat{V}_{ext} + \hat{V}_{int} + E_{II} \tag{1.10}$$

Here $\hat{T}$ is the kinetic energy of the electron and $\hat{V}_{ext}$ is the potential for electrons due to nuclei and $\hat{V}_{int}$ is the interaction between electron and electron and the E_{II} is the interaction for the nuclei with each other.

With the Born-Oppenheimer approximation, the minimum energy configuration is achievable. But with this approximation, it is still difficult to solve the wave function for n^{th} atom.

Hartree-Fock Approximation. Hartree and Fock in 1920 proposed another approximation. In this approximation, it is assumed in a system N body wave function in spite of the product of separate wave function it can be denoted by a Slater determinant of N spin electrons orbitals. In Hartree Fock approximation the electrons orbitals are not dependent on each other. However, this is the drawback and it fails to incorporate the exchange energy. The energy is

$$E = \frac{\psi^* H \psi dr}{\int \psi^* \psi dr} \tag{1.11}$$

The total energy for slater wave function will be:

$$< \psi|H|\psi >= \sum_{i=1}^{N} E_i + \sum_{i<j} (C_{ij} - E_{ij}) \tag{1.12}$$

$$E_i =< \phi_i|h|\phi_i >$$

$$C_{ij} =< \phi_i\phi_j|V_{int}|\phi_i\phi_j >$$

$$E_{ij} =< \phi_i\phi_j|V_{int}|\phi_i\phi_j >$$

Here, E_{ij} is the exchange-correlation between I and J atom and C_{ij} is the Coulomb integral. Another method is LCAO (Linear combination of atomic orbitals) in which molecular orbitals are calculated as a linear weighted summation of individual atomic orbitals.

Density Functional Theory

This theory is based on the ground state density. Many properties can be calculated from the ground state density function. For electronic structure study, this technique is mostly used. In 1964 Hohenberg and Kohn [16] gave this modern formulation of density functional theory. According to this theory, the density of any particles is a basic variable, from which all unique for individual particle's properties can be calculated. In 1965 this concept was further extended by Merlin [17] to finite temperature and grand canonical ensembles. The approach is to generate density functional theory as the theory of many-body systems. For any system of interacting particles, this formalism can be applied. Now the Hamiltonian will be

$$\hat{H} = -\frac{\hbar}{2m_e}\sum_i \nabla_i^2 + \sum_i V_{ext}(r_i) + \frac{1}{2}\sum_{i\neq j}\frac{e^2}{|r_i - r_j|} \tag{1.13}$$

The total energy function for interacting particle system can be written as,

$$E_{HK}[n] = T[n] + E_{int}[n] + \int dr\, V_{ext}(r)n(r) + E_{II} \tag{1.14}$$

$$\equiv F_{HK}[n] + \int dr\, V_{ext}(r)n(r) + E_{II},$$

Here the function $F_{HK}[n]$ includes the potential, kinetic and internal energies for interacting electron system. However, this theorem was not enough for electron structure calculations.

Kohn and Sham in 1965 proposed an ansatz[18] which assumes the ground state's density for an interacting system will be equal to some non-interacting system. This assumption leads to the independent equation of the interacting particle. The complicated many-body terms are now related to the exchange-correlation function of density. The exchange-correlation function became important for the success of the accuracy of the results of the auxiliary system. This theorem is based on the total energy of the function theorem that was proposed by Hohenberg-Kohn. The modified ground state energy function is now,

$$E_{KS} = T_S[n] + \int dr\, V_{ext}(r)n(r) + E_{Hartree}[n] + E_{II} + E_{XC}[n], \tag{1.15}$$

The $T_S[n]$ is the kinetic energy for independent particles. And $E_{Hartree}[n]$ energy is the classical Coulomb interaction energy.

$$E_{Hartree}[n] = \frac{1}{2}\int dr\, dr' \frac{n(r)n(r')}{|r - r'|}, \tag{1.16}$$

If the exchange-correlation potential is known, then one can find the exact ground state energy and density for a system that is interacting.

VASP- The Vienna Ab-initio Simulation Package

VASP is a widely used computer code for calculating the quantum mechanical molecular dynamics and electronic structure calculation from the first principle[19]. It's a plane-wave DFT code that supports LDA, GGA for exchange-correlation energies. For solving many-body Kohn-Sham equations self consistently it uses different potential like norm-conserving, ultra-soft or PAW potential. The algorithms for matrix diagonalization work very efficiently. Even for a small plane-wave basis set. Symmetry analysis reduces the number of degrees of freedom which increases the computational speed. VASP can perform Born-Oppenheimer molecular dynamics also the structure relaxation. Without the need for external data, it can calculate many physical properties by VASP directly.

With the VASP code, molecular dynamics simulation for a few hundred atoms can be performed. However, these runs need very high memory requirements which are tough on regular computers. On regular computers, it would require several weeks for this computation. For medium cutoff energy, a large system of more than 50GB is needed.

Molecular Dynamics Simulation

Another approach for simulating solid is classical molecular dynamics (MD). The benefit is it can treat particle numbers several magnitudes greater than ab initio methods in a shorter time. If a system gets sufficient starting information one can know accurately the behavior of that system by the physical science. Moreover, over can know the exact future behavior if all the relevant mechanisms are known. Classical mechanics is a true example of the above statement[20]. Laplace noted with the mass, position, and velocity of an object, he would give the eternal trajectory for that object. What he meant is solving the Newtonian equation of motion,

$$m_i \frac{\partial^2 r_i}{\partial t^2} = F_i \tag{1.17}$$

$$Fi = -\frac{\partial U(r_1, \ldots., r_n)}{\partial r_i}$$

Where, m_i is the mass and r_i is the position. The force F_i is given as the derivative of potential U. If the correct potential U is known, the trajectory for any small and large object can be deterministically predicted. But then one needs to find n simultaneous differential equations. In practice, the above equation becomes a little more complicated. Instead of trying a set of different equations one usually integrates over a timestep and the position and velocity are being adjusted in each step.

$$-m_i \frac{dv_i}{dt} = \sum_j F_2(r_i, r_j) + \sum_j \sum_k F_3(r_i, r_j, r_k) + \cdots \tag{1.18}$$

$$\frac{dr_i}{dt} = v_i$$

Here F_2 is the force between two atoms and F_3 for 3 and so forth. This problem is much complicated than it looks. One needs to appreciate the problem. The first MD simulation involved 32 atoms with square potential in the simulating phase[21] which was later improved with the involvement of timesteps[22].

But why should classical mechanics work for atomistic behavior? The answer lies between the three assumptions listed below,

1. Even under external forces, the system will settle to an equilibrium state.
2. Any macroscopic event (observable events and parameters) can be described for each atom.
3. The system is ergodic: an average of the ensemble is equal to the average of time. It means, with enough time, a system can reach any microstate.

The last assumption does not mean that any state has the same probability to be reached. It depends on the starting point. There is another unstated assumption that is with time the mechanical energy doesn't change, because of the isolated system. And same things apply for the momentum and angular momentum where non-periodic boundary exists. So, three quantities are preserved: the number of atoms, energy, and volume. That is why it is called the NVE ensemble.

MD simulations afford us the opportunities to assess canonical ensembles with a variety of conditions such as constant volume, controlled pressure (variable volume) as well as controlled temperature. The temperature needs more attention as this very hard to control. It needs to consider the velocity for all particles. This temperature is controlled by the thermostat. The thermostat keeps the temperature of the system the same.

The thermostat is introduced to the system. This is very analogous to a healing bath. This thermostat surrounds the material and controls the temperature.

The temperature in MD simulation is defined by,

$$\frac{KT_{MD}}{2} = \frac{1}{6N}\sum_{i=1}^{N}\sum_{j=1}^{3} m_i v_{ij}^2 \frac{dr_i}{dt} = v_i \tag{1.18}$$

This means, by managing the average velocity of a system under correct distribution the temperature can be controlled. By assigning random velocities initial temperature can be set, so that they fit the Maxwell Boltzmann Distribution. Then for the next step, a simple scheme proposed by Andersen we followed [23]. According to this scheme for each time step, the heat bath interacts with one particle. Then by the Gaussian distribution, the particle's velocity is re-assigned randomly. Once the system reaches the target temperature the speed of convergence becomes sensitive to the frequency collision. The Langevin scheme removes this limitation by introducing the additional force F(t). It works as a noise. But one drawback of this scheme is it sometimes over-corrects.

The solution here is following the Nose-Hoover thermostat [24]. The Hamiltonian is extended with a heat bath becomes:

$$H_{nh} = \sum_i \frac{m_i V_i^2}{2s^2} + U(r,q) + \frac{p_s^2}{2Q} + LKT.logs \tag{1.20}$$

Here, p_s is the momentum of the heat bath variable. If $s(t) = 1$ then the original Hamiltonian can be recovered in the first two terms. Four equation will need to solve the Hamiltonian,

$$\dot{r}_i = \frac{m_i v_i}{s}$$

$$\dot{v}_i = -\frac{1}{m}\frac{\partial \mathrm{U}}{\partial r_i}$$

$$\dot{s} = \frac{p_s}{Q}$$

$$\dot{p_s} = \sum_i m_i s\, \dot{r_i}^2 - LkT$$

The last two terms of the above four equations control the velocity. The controlling equation can also be written as

$$\frac{ds}{dt} = \frac{Lk\left(T - T_{target}\right)}{Q}$$

This equation can control the instantaneous atoms providing a smooth transition. Q here determines the convergence speed.

Now returning to calculating the time integral equation of motion. If one knows the current position for timestep Δt, the next step will be like the following,

$$r_i(t + \Delta t) = r_i(t) + \dot{r_i}(t)\Delta t + \frac{1}{2}\,\ddot{r_i}(t)\Delta t^2 + O(\Delta t^3)$$

Using the negative timestep this expansion will be

$$r_i(t + \Delta t) \approx 2r_i(t) - r_i(t - \Delta t) + \frac{F_i(t)}{m_i}\Delta t^2 + O(\Delta t^3)$$

This algorithm is known as the Verlet algorithm. This is the most commonly used scheme. The computational load is further reduced. The most time-consuming part of this scheme is the calculation of the force [25] expressions. So, separation of short-range and long-range forces can help to mitigate this problem. If the forces only in some range are considered then one can reduce the consideration of $N_{neigh} = \frac{4\pi}{3}\rho r_c^3\ neighbours.$ This is called the cut-off range. Including this in the Coulomb interaction which is very used to interaction for the biological and ionic system. In that system, interactions can be found in every pair. A system containing n-body system will n^2 interactions that turn up the computational costs

with increasing n. So, considering only a certain range helps here, and most energy or interesting interactions are contained with a reasonable choice of r_c.

Here let's talk whether the atom's point mass treatment is justifiable or not. De Broglie wavelength can be calculated quickly which gives a rough limit for quantum effect, for most atoms this wavelength is .2 A^o at room temperature. This value is far below than the general atomic distance (1-3 A^o). Thus, one can ignore the quantum effects safely provided it's not for light atoms and not for very high temperature.

Another is being cautious about the limit of length scale and time involved. Even for a run with a million steps, it would take only several nanoseconds. This sometimes makes confusion as sometimes strain might take 10^{-4}/ps but this would translate to a rate 10^{8}/s. And also, the number of atoms is limited to scale millions. Periodic images for homogeneous systems can be used to mitigate this problem.

The timestep is the third issue. The size of the timestep is the inherent parameter for the Verlet algorithm. Choosing a smaller step size would make the calculation longer.
Lastly addressing the atomic interaction issues. CMD needs potential energy because it needs instantaneous electron adjustment. So chemical bond breaking and forming are not needed in the simulation.

So, most importantly one needs potential energy for running CMD. This could be obtained by fitting the parameters like volumes, pressure, many more mechanical properties from experimental data or ab-initio calculation into the appropriate relations. This is a very time-consuming process and for many elements, the availability of potential is more tough. The system with more than two elements makes things more complex. And this process is very sensitive to the input data which means one potential for a particular structure consisting of the

same elements but with different structures might not work satisfactorily outside its original design. This is called transferability which is also a priority checklist for developing potential energy. Developing the potential for CMD is the objective of this study.

Comparing the ab-initio simulation with MD simulation from the above discussion, there are few basic differences. The length scale and time for the calculation for MD simulation exceed ab initio simulation by a far big number. A sketch is shown in Figure 3, comparing these scales,

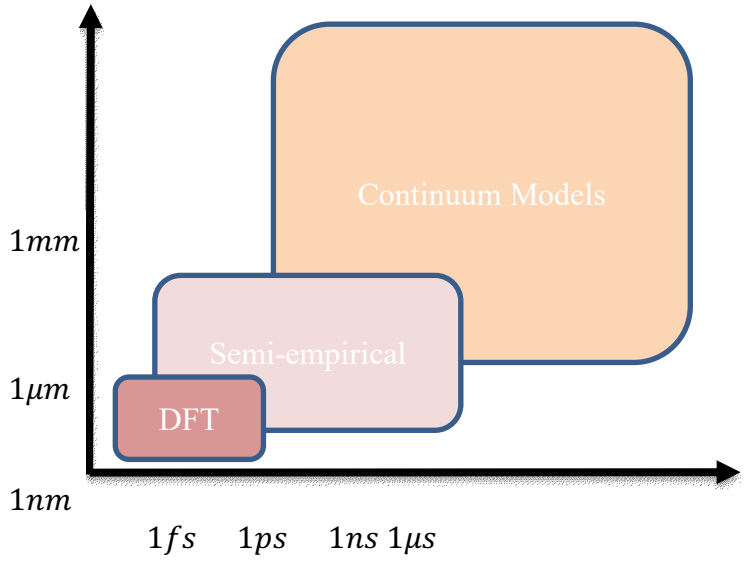

Figure 3. Different simulation methods based on time and length scales.

Ab-initio method is for system sizes around a few nanometers and time for the simulation is picosecond. It can handle only a few hundred atoms but Semi-empirical method CMD can handle a billion atoms for few nanoseconds.

Due to simplicity, CMD has become a popular simulation. There are many codes for CMD, LAMMPS[26], Camelion, IMD, MDACP are some choices. Among them, LAMMPS is

the most popular. And there are some that are used biomolecular processes like NAMD, CHARMM, and AMBER.

Embedded Atomic Method. The need for the reliable interatomic potential for classical molecular dynamics was discussed in the previous section. Ab-initio molecular dynamics depend mostly on the electronic structure of elements and Classical molecular dynamics depend on the accurate behaviors and representing observable parameters. In the following sections, the general idea of the EAM potential and the reason behind considering this potential method over many more potentials will be discussed.

Basics of Potential System. How atomic interactions should be represented is the major question in atomic modeling. With effective potentials, there were several attempts to represent many-body interactions. In a simple model, atoms are made of positively point charged particles with negatively charged electrons surrounding it. This is why atoms follow electrostatic potential. This core comprises the vast majority of atomic mass. And this core will have an outsized contribution to the interatomic relation. And this positive charge will have an explanation of the separation between atoms as a repulsive and attractive force.

Pair-potential might be successfully used for inert impurities in metals like He [27] because it is effective for chemically active impurities, but it fails to represent the energy of H in the transitional metal cluster [28]. But such a simplistic view will not give the proper picture of the interaction between the atoms. As an example, atoms would not come to close each other unless there is unrealistic high energy involved and also atoms would not go any direction. If it would happen then any structure formation would be impossible. That is why the attractive and repulsive both forces are acting as a relation between core and electrons. And between this

attractive force and repulsive force, there is an equilibrium position that is the resting position for an atom. And this is reflected as regular crystal spacing.

And dwelling over the exact nature of the interaction would be very time consuming and overly complicated and would involve a huge amount of time just for defending the quantum mechanical phenomenon involved. I would also avoid describing the fine details of the atoms because this might impede the generality of the model. Simply as the basic form, a combination of repulsive and attractive behavior will express the interatomic potential, and this is known as pair potential.

There are some basic features that should be satisfied for a pair potential to be applicable to as many systems as possible. Firstly, the distance should be the primary variable. For example, in an isolated where there is the presence of outside force and there are only two atoms in the system, the energy will come from the interatomic potential. And, as there are no other atoms in the system, radial symmetry is achieved, this means the system ought to be constant with rotation. So, the only variable that would affect the energy is the distance in a spatial sense. Secondly, as mentioned before atoms should not come arbitrarily close by means of repulsive force. This will lead to a rational function. Third, as in regular crystal structure, the function should have an equilibrium position. And this is not only allowed for the two-body system, but this is also allowed for the noble gas system too. And with increasing separation the interaction energy should vanishes. As mentioned before, for the isolated system the separation grows, and the system will become more like a simple system of charges. And lastly, the pair potential should be a smooth function. The function should be continued until the second derivative. This will ensure any unphysical behavior will not hamper the potential, as the real-life forces do exist in continuous form everywhere.

Many functions surprisingly satisfy these above-mentioned conditions. Most of them have the rational function r^{-k}. And this satisfies the second property. The earliest example would be the Lennard Jones potential which was derived from the gas equation of state.

$$V_{LJ}(r) = \varepsilon\left[\left(\frac{\sigma}{r}\right)^{m} - \left(\frac{\sigma}{r}\right)^{n}\right]$$

Here, σ is positive and both attractive and repulsive forces are represented. Here, $\sigma, \varepsilon, m, n$ are variables that should be determined fitting and values of these parameter varies from one atom to another. It should be mentioned that this was the first empirical potential. Unlike Coulomb's potential and its variation, in this Lennard Jones potential variables $\sigma, \varepsilon, m, n$ do not have the information about the atom itself. And this would be an important feature. With the system getting more complicated, these parameters would fit on some other independent data.

Other functions are also there. One of the simpler types is Morse potential. Morse potential was formed for harmonic oscillator approximation. It can be written as

$$V_{Morse}(r) = D_e\left[1 - \exp\left(-a\left(r - r_{r_e}\right)\right)\right]^2$$

It has a unique feature, the equilibrium distance r_e is specifically prescribed which comes from the second derivation of this equation. This function is not for any particular interaction of a model but it performs well for the harmonic oscillator model.

Another improvement of Lennard-Jones is Buckingham Potential,

$$V_{Buck}(r) = Aexpt(-Br) - \frac{C}{r^6}$$

This potential was designed for classical gases, for example, noble gases. This is a very common scenario that the general forms can not accurately represent the increasingly complex

system. There is another pair potential that was designed for the crystalline system of metal and this is also empirical oscillating pair potential. This function represents

$$V_{eopp}(r) = \frac{C_1}{r^{\eta_1}} + \frac{C_2}{r^{\eta_2}} \cos(kr + \phi)$$

This function also contains the long-range behavior of oscillation that is found in transition metal [29]. This is why it is very useful potential for the work I am working on. The variable, φ does not depend on the angular phase. More context about this potential will come in the next chapter.

Improvements in Pair Potential. So far, I have discussed extensively the basic form of pair potential function. And as mentioned, the repulsive and attractive behavior of the forces has to be smooth. But considering only the pair potential would not suffice for the proper representation. For example, let's consider a system containing the carbon molecules and if the system is restricted to have a 2-dimensional system like graphene. Even with this simplest system atoms will not take any prescribed equilibrium position. They can take hexagonal, pentagonal or any kind of shape. This phenomenon is called covalent bonding and it happens because it has a preferred direction, an angular dependency instead of the traditional picture. This angular dependence is overlooked by pair potential. This was the first suggestion for a change in the pair potential.

But one thing to be remembered, that for ab-initio calculation, none of the change will take place in the pseudopotential model. The pseudopotential thinks atoms in a system as an individual entity consisting of two parts: nucleus core and valence electrons. It does not see the other atoms it's interacting with. The approximation of the wavefunction is calculated by applying the boundary between the atoms. Pseudopotential's form tends to mimic the real behavior of the atoms like the directional bonding.

Now, the potential system can be classified into two sections, one having the pair potential and the others that do not use the pair potential. The systems that use pair potential, its major energy component depends on the pair interaction though for reflecting a certain behavior additional terms must come in the energy landscape favoring some specific configuration. For example, Embedded Atomic Method (EAM) considers a new term called embedding energy[30]. Embedding energy shows the contribution of electron density with its neighbor. And more improvement came to it with the addition of Angular dependent Potential (ADP) [31]. This ADP represents the dipole and quadrupole contributions. And this angular dependency causes deviation from a specific structure to a more favorable structure. The potential that does not consider pair potential for favoring a more complex system still keeps the pair potential principle in the formation. An example would be Tersoff potential [32], is made of both attractive and repulsive function, here this is different than the usual pair potential because the attractive force considers triplet instead of just a pair. This considers a third atom has an effect on the former bonding with a particular angle. An improvement of this Tersoff potential is the Analytical Bond Order Potential [33]. In this scheme it does not only take care of three body potential but also the bond order. Specially the number of chemical bonds among two elements. But these models are not widely used to describe metals. Some might give us favorable results for metals but in general, these are not perfect for metals. Only EAM potential is the one that is widely used for describing metal.

EAM Potential. As mentioned, many times before only pair potential cannot be enough to define a metal's Interactions. Though its simple and useful for many cases but for metal it hits limitation very quickly. Another fact pair potential can be used for fitting bulk properties, but it fails to handle a structure of less perfect crystallinity. As an example, for grain boundary. That is

why a different robust approach is needed here. One approach is solving DFT calculation for solving the Schrödinger equation. But this is highly impractical. This problem can be simplified by assuming the cohesive energy which can be written as

$$E_{coh} = \frac{1}{2} \sum_{i,j;i \neq j} V(r_{ij})$$

The cohesive energy is some of the bond pairs and these bond pairs are not dependent on each other. Some metal has two phases fcc and bcc which have different properties based on the phases[34]. It suggests the coordination number has an effect on it, so the independent each bond will not suffice.

So new modification should be added for accounting the coordination issues. This is important for low symmetry structure problems. And for dislocation cases, grain boundaries system and even the quasicrystal system it's very useful. And also, a different form can be added to pair potential for accounting bulk of the binding energy, thinking that it would be a course correction to the pair potential. Considering all of this the energy in EAM was written as[35],

$$E_{coh} = \frac{1}{2} \sum_{i,j;i \neq j} \emptyset_{ij}(r_{ij}) + \sum_{i} F_i(\sum_{i \neq j} \rho_j^a(r_{ij}))$$

Here, r_{ij} is the atomic distance between the i-th and j-th atom, $\emptyset_{ij}(r_{ij})$ is pair potential function. $\rho_j^a(r_{ij})$ is the electron density of the i-th atom due to j-th atom. $F_i(\sum_{i \neq j} \rho_j^a)$ is the embedding energy.

Here I will discuss more about embedding energy. The embedding energy F_i is the Interaction of the i-th atom at its nucleus electron gas in the background. This background gas is the contribution of the other atoms of the system as an atom is embedded to a location with the host of electron density. This makes sense cause; metal is constituting of electrons sea on the surface. Most of the cases it is complicated to describe the host-atom interaction, it cannot be

described just through certain types of bonds. This function considers the contribution from all atoms as a many-body interaction. Some simple modifications were done. One, the electron density is considered as embedded by individual contributions. And this model can represent any kind of delicacy like accounting for different properties of different phases and also it can represent any coordination. The density term holds all of these detailed delicacies. This is why EAM potential is very popular.

One thing is to notice that, this formula is not unique for EAM potential only. Some other schemes have similar ideas or even further addition to this idea. For example, Finnis-Sinclair N-body potential [36] would have an idea similar to EAM potential. The only difference is, it has more physical additional terms. But it allows the embedding energy in a different interpretation. The ADP model that was discussed before has the form,

$$E_{coh} = E_{EAM} + \frac{1}{2}\sum_{i,\alpha}(\mu_i^{\alpha})^2 + \frac{1}{2}\sum_{i,\alpha,\beta}\left(\lambda_i^{\alpha\beta}\right)^2 - \frac{1}{6}\sum_{i} v_i^2$$

The last three terms are multiple expansions of the force cubic system. Another improvement of EAM potential is the Modified Embedding Atomic Method (MEAM), which was proposed by Baskes [37]. This scheme does not favor any specific cubic structure. This function is quite similar to the equation of EAM, but the density function varies by angles and it does not take the average over the equidistant sphere. For directional bonding, MEAM is more useful than EAM. This is the reason for a system containing covalent bonding MEAM if more useful than EAM [37], also for intermetallic alloy [38] and for ceramic TiN [39].

One thing to notice is in the pair potential there is no mention of the structure of the pair potential, embedding energy or electron density function. The pair potential is the variation electrostatic energy,

$$\emptyset_{ij}(r) = \frac{Z_i(r).Z_j(r)}{r}$$

Here Z_i, Z_j are charges of the atoms i and j. Moreover, the pair, embedding and density function are fitted so that they follow some basic properties like bulk modulus, vacancy formation or elastic constants. Some functions are later modified or omitting [30] highly simplified interaction but at the same time imposing function for exponentially decaying convex on the density. These approaches make sure that all the important parameters are intact while producing the potential. This way one can get accurate data that match experimental results and it prevents to have any unphysical behavior. But one downfall might be is the transferability due to the too much dependence on the bulk property of the structure.

To get around this problem, new force-fitting codes like Potfit [40], MEAMfit[41] use reference-free method. In these codes, the accurate forms of desirable function are fitted freely. Instead of considering physical properties like bulk modulus, it considers two distinct atom species and tries to fit it. This fitted function is smooth and can fit more inputs which makes it more flexible. One can get the desired phenomenon by tailoring the inputs but at the risk of allowing unphysical behaviors. This one problem one should be careful of while fitting. Again, reference-free method removes all the constraints on fitting parameters which leave the issue of maintaining reasonable behavior to the functions. Like, if it is not prohibited, the four criteria should be satisfied by pair potential. Efforts have been made for finding universal form [42] but at the end, one should focus on the properties specific structures so that function can reproduce the structure again.

Modified Embedding Atomic Method

The force-fitting code that I used in this research is MEAMfit (Modified Embedding Atom Method) [41]. Though our focus is developing the EAM potential but the force code MEAMfit is more popular for developing the MEAM potential. To describe how MEAMfit works let's look at the total energy within the RF-MEAM formalism,

$$E = \sum_{i=1}^{N} E_{\alpha_i}^{emb}(\rho_i) + \frac{1}{2}\sum_{i\neq j}^{N} \phi_{\alpha_i\alpha_j}(r_{ij})$$

$$E_{\alpha}^{emb}(\rho) = \alpha_{\alpha}\rho^{\frac{1}{2}} + b_{\alpha}\rho^2 + C_{\alpha}\rho^3$$

$$\rho_i = \frac{2\rho_i^0}{1+e^{-T_i}}$$

$$T_i = \sum_{l=1}^{3} t_i^l \left(\frac{\rho_i^l}{\rho_i^0}\right)^2$$

Here, $\phi_{\alpha_i,\alpha_j}(r_{ij})$ denotes the pair potential between the i^{th} and j^{th} atoms with r_{ij} distance, $E_{\alpha}^{emb}(\rho_i)$ is the embedding energy where ρ_i is the electron-density at site i, ρ_i^0 is the sum over electron densities.

$$\rho_i^0 = \sum_{j\neq i}^{N} f_{\alpha_j}^0(r_{ij})$$

Where $\rho_i^{l>0}$ are angular contributions to the MEAM approach, and for EAM potential it is set to zero. This presents bond-angles (θ_{jik}) into the formula.

$$\left(\rho_i^l\right)^2 = \sum_{j,k(\neq i)}^{N} f_{\alpha j}^l(r_{ij})\, f_{\alpha k}^l(r_{ik}) P^l(cos\theta_{jik})$$

Where $f_{\alpha_i}^{l>0}$ is the partial electron density contributions and P^l(l=0,…,3) are Legendre polynomials. The partial electron densities

$$f_{\alpha_i}^{l}(r) = \sum_{n=1}^{4} a_{\alpha_i}^{n,l}\left(r_{\alpha_i}^{n,l} - r\right)^3 \theta\left(r_{\alpha_i}^{n,l} - r\right)$$

$$\phi_{\alpha_i,\alpha_j}^{l}(r) = \sum_{n=1}^{4} b_{\alpha_i,\alpha_j}^{n}\left(S_{\alpha_i,\alpha_j}^{n} - r\right)^3 \theta(S_{\alpha_i,\alpha_j}^{n} - r)$$

Here $a_{\alpha_i}^{n,l}$, $b_{\alpha_i,\alpha_j}^{n,l}, r_{\alpha_i}^{n,l}$ and $S_{\alpha_i,\alpha_j}^{n}$ are the parameters that need to be optimized. For pair potential form distance r is more than 1.5 $A°$ and for less than 1.5 $A°$ this pair potential will take the form of Ziegler-Biersack-Littmark [43] style.

Energies and forces from DFT calculations are fit by MEAMfit code. Fitting data comes from the vasprun.xml files produced by VASP. For running for the first time MEAMfit generates fitdbse file which contains the trajectories. One needs to adjust these files according to the specific requirements. The optimization function that MEAMfit minimizes is given below:

$$R^2 = \frac{\sum_n W_n\left(E_{pot}^{n} - E_{DFT}^{n}\right)^2}{\sum_n W_n\left(E_{DFT}^{n} - E_{DFT}^{avg}\right)^2} + \frac{\sum_n \sum_{i,\beta} W_n\left(F_{\beta,pot}^{n,i} - F_{\beta,DFT}^{n,i}\right)^2}{\sum_n \sum_{i,\beta} W_n\left(F_{\beta,pot}^{n,i} - F_{\beta,DFT}^{avg}\right)^2}$$

Here n runs all structures specified in vasprun.xml files. E_{Pot}^{n} and E_{DFT}^{n} denotes the total energy from the generated potential and from the DFT data for n^{th} structure. Same for $F_{\beta,i,pot}^{n,i}$ and $F_{\beta,i,DFT}^{n,i}$ which represents the force from potential and ab intio data. β denotes the cartesian components on atoms i of n^{th} structure. And W_n represents the weight which gives relative importance to the quantities of the fitting database. A value of R=0.1 tells the error in EAM energies equals to 10% of the ab-intio data.

MEAMfit follows the conjugate gradient algorithm (CGA) and genetic algorithm (GA). CG algorithm is used for minimizing the R. First potential is developed by initializing every potential parameter randomly within the prescribed bounds. For pairwise coefficients, t_i coefficients and energy offset are randomly seeded in the range [-10,10]. Random values are

generated for cut-off radii in the pairwise functions. These random values come from the smallest interatomic distance of fitting database (0.9 *A*°) and the maximum cut-off radius mentioned by the user. Once the minimization starts and the value R comes below 10 the randomly seeded potential will go for CG-optimization. The initial vetting takes around 20s but improves the optimization function. Once 10 potential is generated using this approach, GA is used to randomly combine pairs of potentials.

Using GA allows getting the global minimum which is tough to get just from the randomly seeded potentials. This optimization allows learning from past optimizations.

Though the first value of the potential parameter is generated randomly, one can use the existing potential to set up these starting values. In the setting file, POTFILE=potparas_in MEAMfit can get the starting values for the subsequent optimization. Once the optimization is complete MEAMfit produces EAM potential in LAMMPS format and CAMELION format.

COMPUTATIONAL DETAILS

Ab-initio Details

The most sensitive part is the sampling of the force and energy data to accurately model the EAM potential. These samples are a very crucial parameter for the force-fitting. In this section, computational details for generating these samples will be discussed.

Sample Structures:

As our main target was to develop the interatomic potential for Ni-based superalloy so for the beginning, I selected a structure that has the two main elements of the superalloy. And that is Ni and Al elements but also, I wanted to have a structure that has more Ni than Al. I specifically selected FCC ordered Ni3Al structure here as this structure is Ni-rich which would serve our purpose.

I used the Open Crystallography Database [44] for obtaining the Ni3Al structure. The lattice parameter for this structure was 3.56 *A*°. This structure (Figure 4) was then been made supercell of 3 × 3 × 3 by Ovito[45]. The number of atoms was 108, Ni 81 and Al 27.

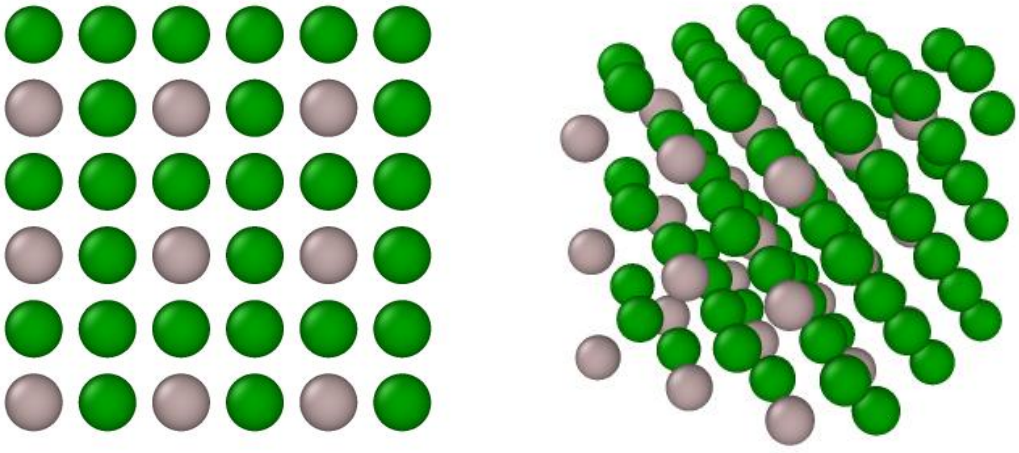

Figure 4. . Front view (left), Perspective view (middle), Top view (right) of Ni3Al

I also used the slab for getting the ab-initio data for gamma-gamma prime structure ($\gamma\gamma'$). For creating this slab, I used the unit cell again to make it supercell with $6 \times 2 \times 2$ and deleted the Al atoms from both ends of this structure, thus created $\gamma\ structure$ at both end. The number of the atom was 96 among them 84 was Ni atom and 12 was Al atom. The middle portion of this slab represents the gamma prime phase (γ') and the two sides represent the gamma phase (γ) in Figure 5.

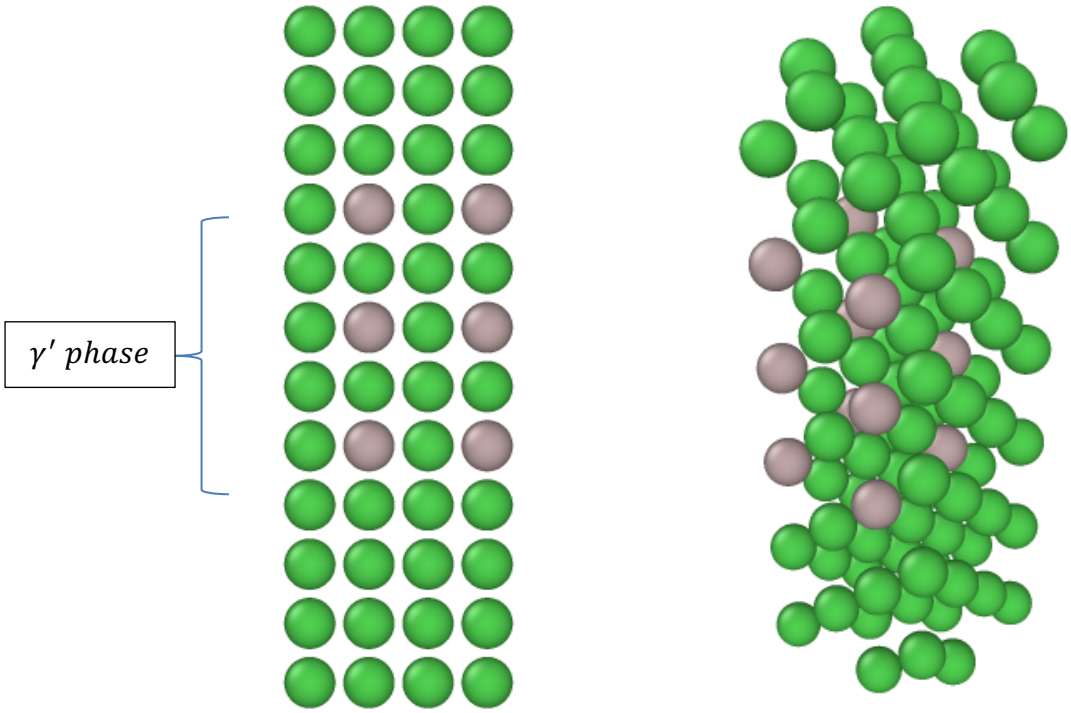

Figure 5. The slab of Ni3Al structure. Left front view and right the perspective view.

The vast calculation can be very time consuming depending on the parameters, so we restricted our structure to have too many atoms. But again, in the NPT run, it is suggested to have more cells which are needed for catching different vibrational energy. In some of the runs like Cij which does not need any supercell to produce the appropriate force data, we selected only unit cells.

For the Carbide system, I took three different structures of Carbides: Mo23C6, W23C6, and Cr23C6 (Figure 6)

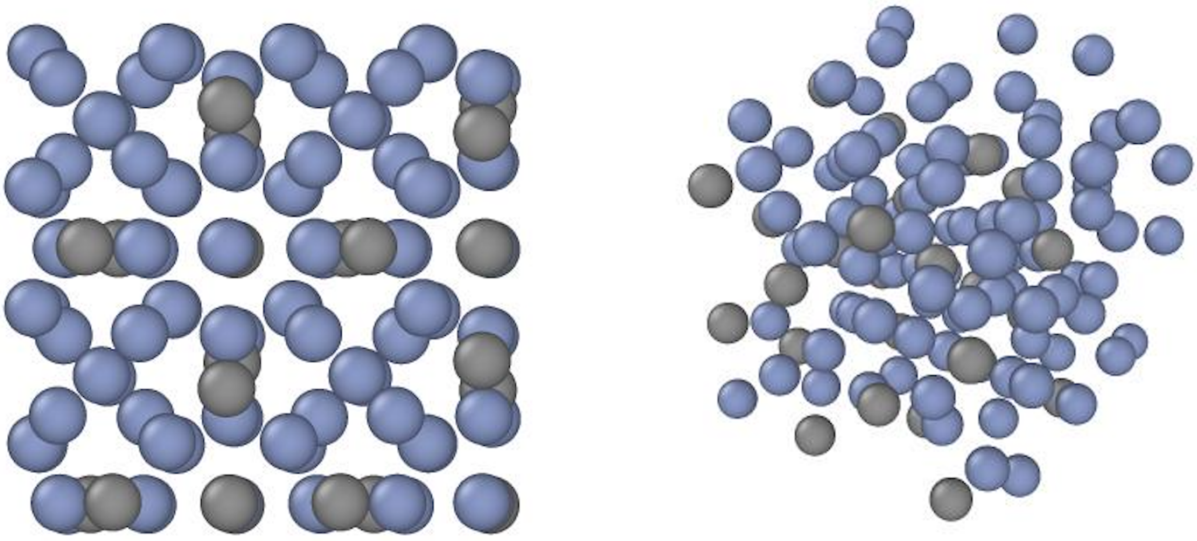

Figure 6. Relaxed structure of Cr23C6. Front view (left) and Perspective View (Right)

This structure for Cr23C6 was obtained from the material project website [46]. The number of the atoms was 116, Cr was 92 and C 24. The space group of this structure is $Fm\bar{3}m$ and the lattice of the unit cell is 3.517 A^o. The other two carbides were obtained from this same structure just replacing all Cr atoms with the targeted atom, Mo or W. So, for both Mo23C6 and W23C6 the number of atoms, the lattice constant, space group was exactly.

Simulation Procedure:

In this section, I will discuss the simulation process for calculating the ab-initio data. The above structures were simulated with first-principle calculation. And thus, the critical information of force and energy was obtained. The Vienna Ab-initio Simulation Package (VASP) code [19] was used for this ab-initio molecular dynamics (AIMD).

In the ab-initio calculation, the objective is to get a dynamic range of Cartesian force data and with the relatively least computational resource. Here I tried to give atoms sufficient movements from their stable positions and this trigger variations in the energy and force. So, I subsequently varied the force by triggering the movements and that helped for developing EAM potential. There are many ways that can attain different forces and energy information. I first reached this goal by simulating the structure at different temperatures. Generally, the idea is to get a smooth transitioning in force sampling. That's is why instead of jumping to the very high temperature, I started from room temperature and increasing it to so far close to the melting point. This method worked well before in quasi-harmonic behavior of high-temperature binary ceramic[47][48]. So, we followed that approach by simulated temperatures at 300K, 500K, 700K, 1000K and 1500K for Ni3Al structure. One benefit of having low temperatures sampling is that it helps in the faster convergence of parameter.

Pair potential is a very important part of defining the EAM potential. For training the data that could resemble the pair potential in the system another approach, changing the volumes of the structure, was followed. The idea is if the volume of the structure is shrunk and expanded then the samples will have information about force interaction with a different distance of the atoms. So, the Ni3Al structure was shrunk and expanded from its most stable structure. After getting the supercell the structure was relaxed by ground-state calculation and then the structure

was shrunk by 2% till it shrunk by 10% of the original structure and also expanded by 2% till it expanded to 10%. So here, 11 different structures were made. And then ground state calculation was done one each of this structure.

The POTCAR which represents the pseudopotential for every atomic species was obtained according to VASP recommended PAW potentials [49]. The ENCUT was kept high to capture predominant vibrational modes for Ni3Al at high temperatures. Though low encut (240 eV) was suggested for Ni3Al, but I chose 520 eV for these runs. $3 \times 3 \times 3$, Monkhorst-Point k points sampling was used for the calculation efficiency for all of the structures. GGA exchange-correlation function was used. The self-consistent field convergence was set 5E-6 eV/atom.

The first run I did was the ground state calculation which relaxed the structure for all the consecutive runs. Then for NPT runs Langevin thermostat was used and the pressure was set at .0001Kbar. For Cij calculation only the unit cell was used instead of the supercell for the computational efficiency. All the other parameter was kept the same. For analysis and visualization

Purpose, VMD code [50] was used.

For the Gamma-Gamma Prime slab structure instead of doing just the NPT, NVT runs were done. Because with NPT runs the average pressure comes very close to the 0 but my goal was to create more pressure which might create more energy. So, the goal was to get an average 1300Kbar pressure from the VASP output. But as the NVT runs with the same precision mentioned above failed to achieve targeted average pressure, I shrunk the structure by 10% from its original position and again ran the NVT runs with different temperatures of 1000K, 1500K and 2000K. This makes the average pressure for all of the individual runs more than 1300Kbar.

For the Carbides, in the same way, all of the NPT, NVT runs were calculated. As the Carbide has a high melting temperature so for both NPT and NVT runs were done up to 3000K. Unlike Ni3Al, in carbides, I did not change the volume of the structure for getting different energy data as the average pressure that was obtained from the carbides NVT runs were near to 1800Kbar which was already high. The Encut were kept higher than the recommended VASP values for all of the runs. And all the other parameter was kept as high precision.

Force Fitting. The next step was to produce the EAM potential through force-fitting code, MEAMfit [41]. MEAMfit uses the force, energy and stress information generated from the ab-initio calculation and fits those data to a chosen potential model for getting the potential. Details of how MEAMfit works were discussed in the introduction part.

Fitting Procedure. After running the VASP package several outputs were generated for each of the structures. MEAMfit uses the vasprun.xml file from the ab-initio. This file contains all the necessary information about force, energy and stress information.

The first important task was the labeling of each of the vasprun with a unique name so that later it can be organized properly for the fitting process. Gathering all the necessary vasprun.xml files the MEAMfit code was run for the first time. This run generated a file named "fitdbse" and then terminated.

In the fitdbse all the vasprun files were listed with their no. of trajectories. For the ground state samples I kept all the trajectories for the runs but for NPT runs it was suggested to eliminate the first 10-20% trajectories as those trajectories might not have the appropriate force information for the particular temperature. So, for all NPT runs either I chose the last 10 trajectories and in some cases more. As MEAMfit also allows us to skip some trajectories and take selective trajectories for each fitting points. So, for a few runs, I chose "s5" to take every 5^{th}

no of trajectories for a more dynamic range of trajectories. I will list out the selection of trajectories for each run in the result section.

From the third column, one can select the type of energy and the weights for the individual optimization function. As a default, it was free energy with only energy optimization. But for all of our run, I chose total energy with all the three factors (energy, force, and stress) selected. In some of the runs, only free energy with energy optimization was selected.

After correcting the Fitdbse file, MEAMfit was run again which generated the setting file. Here one can choose which potential to create an EAM potential was chosen in my runs. For the CUTOFF_MAX which determines the radius of cut-off radius I selected $7A^o$. For selecting this value, I used the radial distribution function for the relaxed structure. The radial distribution of Figure 7, gave us the distance for the 5th nearest neighbor distance which was 7 $A°$.

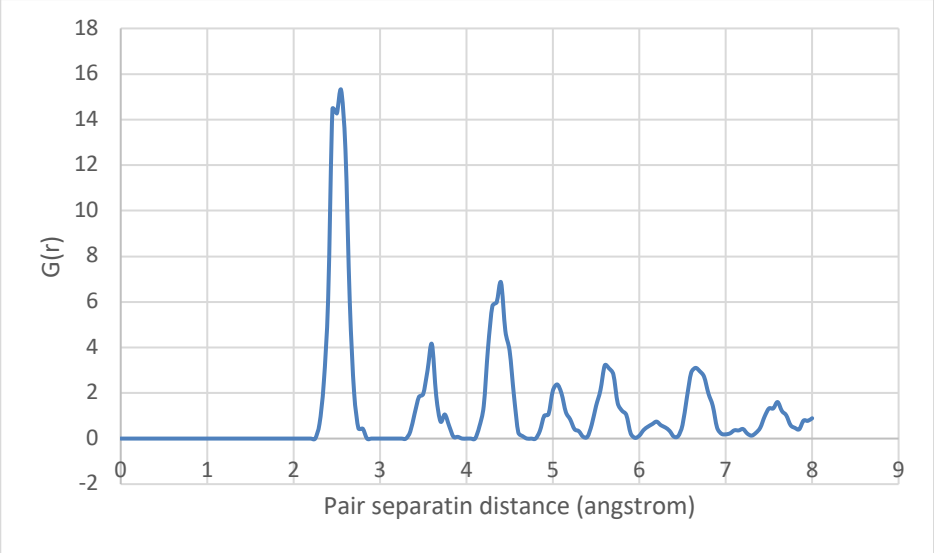

Figure 7. Interatomic separation plot for the relaxed structure of Ni3Al.

Selecting this value for the CUTOFF_MAX would develop an EAM potential for which 5th neighboring interaction was included. The next two terms determine the pairwise terms in the expansion of pair-potentials and electron densities. I chose 3 for both of these terms. For the

OPTFUNCTION which determines the threshold for CG (conjugate minimization) during the random sampling process, I selected the default value 10 for computational efficiency. Every time MEAMfit produces an EAM potential it generates also a file named Potparas_best file which contains the existing potential parameter. The very fast run was done from scratch but for the next MEAMfit runs I used the previously created Potparas_best file to use as a starting point while optimizing and it saves a lot of time.

Generally, one successful optimization for my selected system took 12-14 hours on average. But one should wait for a complete optimization message. Although sometimes in my runs even after 127hr the optimization kept going. In those cases, I noticed even after multiple successful optimizations, the optimization function did not improve. So, based on the improvements in Optimization function F, I decided to terminate the runs or keep going.
After each run, analysis like structural stability and mechanical properties and transferability were checked for each EAM potentials. If the potentials were failed in analysis, more samplings according to the need were generated through ab-initio and then it was fitted again unless until it satisfies a certain scale of the analysis.

RESULT

Ab-initio Molecular Dynamics

DFT calculations were carried out on every sample with various temperatures and compression levels. The runs were done for enough time so that for each time we get enough trajectories (more than 50 at least) for NPT runs. For NPT runs it was checked whether it came to a stable targeted temperature and also for NVT. The scripts for ground state, NPT and NVT calculation can be found in appendix.

In Figure 8, I present the radial distribution function at different temperatures and at different pressure. As discussed before the reason for having the NPT run at different temperatures is to generate samples with large variational atomic configuration.

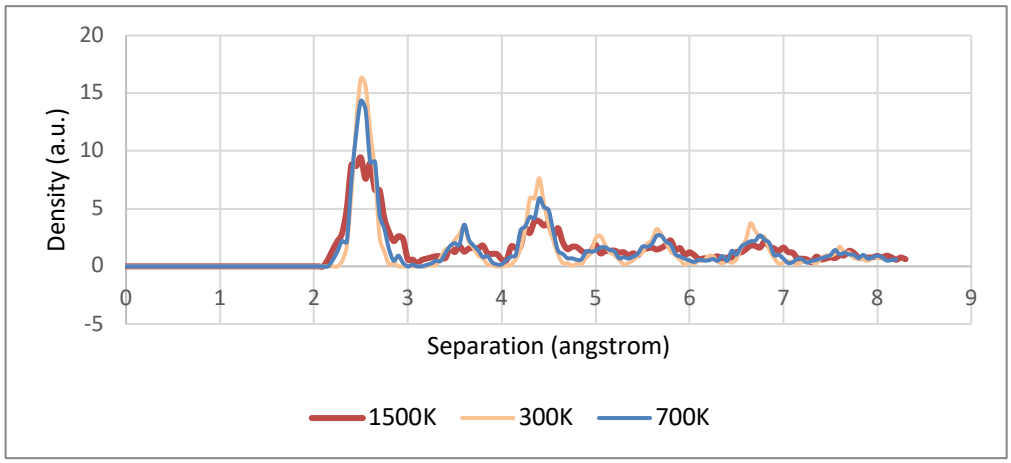

Figure 8. Radial Distribution for different temperature simulation for Ni3Al

From this graph, it was concluded that with the increase of temperatures in the NPT runs the peak of the RDF plots getting broadened. It means with more temperatures more accentuated forces were created.

And the same things were expected from the different volumes ground state samplings. With decreasing volume structure more prominent and larger forces can be achieved as we can see from Figure 9. And this approach seems to work well.

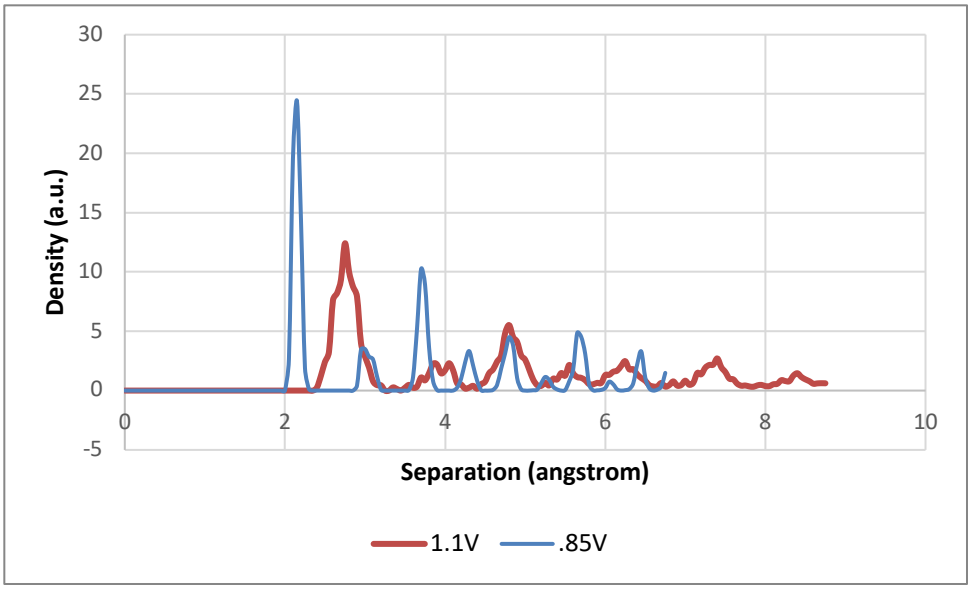

Figure 9. Radial Distribution for different volumes simulation for Ni3Al

With increasing compression peaks are getting higher and also shifted to the right. Thus, variation in the atomic arrangements was got. Though shifting of the peaks tells us that the compression lowers the length. It suggests the unoccupied space is reduced dramatically. And atom movements during the MD simulation are restricted. And after a certain point atom, movement restriction will be overweighed by the extending compression level which will create artificially stagnant configurations. Another problem is that very high pressure slows the convergence of the run which leads to a significant increase of time to reach the targeted equilibration. In spite of that, these data are deemed to work well for force-fitting purpose to generate MD potentials.

Lots of DFT calculations were done for creating the sample based on the need but here I will discuss only those were used in the EAM potential that I am going to discuss in the next

chapters. The total number of samples that were used for our force fitting for Ni3Al is 21, among them 12 is different ground state samples, 5 NPT runs having more than 200 trajectories in each, 1 Cij sample holding 37 trajectories, 3 different NPT runs for gamma-gamma-prime structure. After creating the Cij sample, I checked the validity by comparing each of the elastic constants with the ideal values for this crystal structure from the material project website. Because these inputs are very sensitive for creating the EAM potentials. That's why initial input for the Cij sample was checked every time in the DFT calculation and fine-tuned in the parameter until its results match the reference value from the material project's website which has been shown in Table 1.

Table 1. Comparison of elastic constants from ab-intio with ideal elastic constants

	From ab-inito (GPa)	Reference value (GPA)
C11	227	238
C12	138	147
C44	126	129

The elastic constants that were calculated through the first principle for the cubic system, should also satisfy the following mechanical criteria[51],

$$C_{11} - C_{12} > 0$$

$$C_{11} > 0;$$

$$C_{44} > 0;$$

$$C_{11} + 2C_{12} > 0$$

Values obtained from the ab-initio data satisfied these criteria. And also, these values are very close to the reference values which verifies these data.

Developed EAM_Potential through MEAMfit

Several EAM potentials were generated through MEAMfit. In Table 2, all the produced EAM potentials are listed.

Table 2. lists of the EAM Potentials with the samples that were used.

	EAM_Pot_1	EAM_Pot_2	EAM_Pot_3	EAM_Pot_4	EAM_Pot_5
Samples Used	11 ground samples of different volumes	1 Ground state sample of the equilibrium position and 1 NPT sample (300K)	1 Ground state sample of the equilibrium position and 5 NPT sample (300K, 500K, 700K, 1000K, 1500K)	11 ground state sample and 5 NPT samples	All the samples from EAM_Pot_4 with 1 Cij sample

In the next chapter, this table will be referred a lot, because based on these samples, the results of the analysis varied, and which ultimately guided me to different approaches.

Every time potential is generated, the quality of the fits was seen by comparing energy and force from the ab-initio simulation with energy and force from MD simulation of the created EAM potentials. The ab-initio force and energy are called the true data and the one from EAM

potentials are called the fit data. A perfectly converged potential will reproduce the same data as the input. Thus, if one plot the true data vs fit data it will create a straight line having a slope of 45^o. And also gives another value called optimization function F, which gives the idea of how well a potential was fitted (Figure 10).

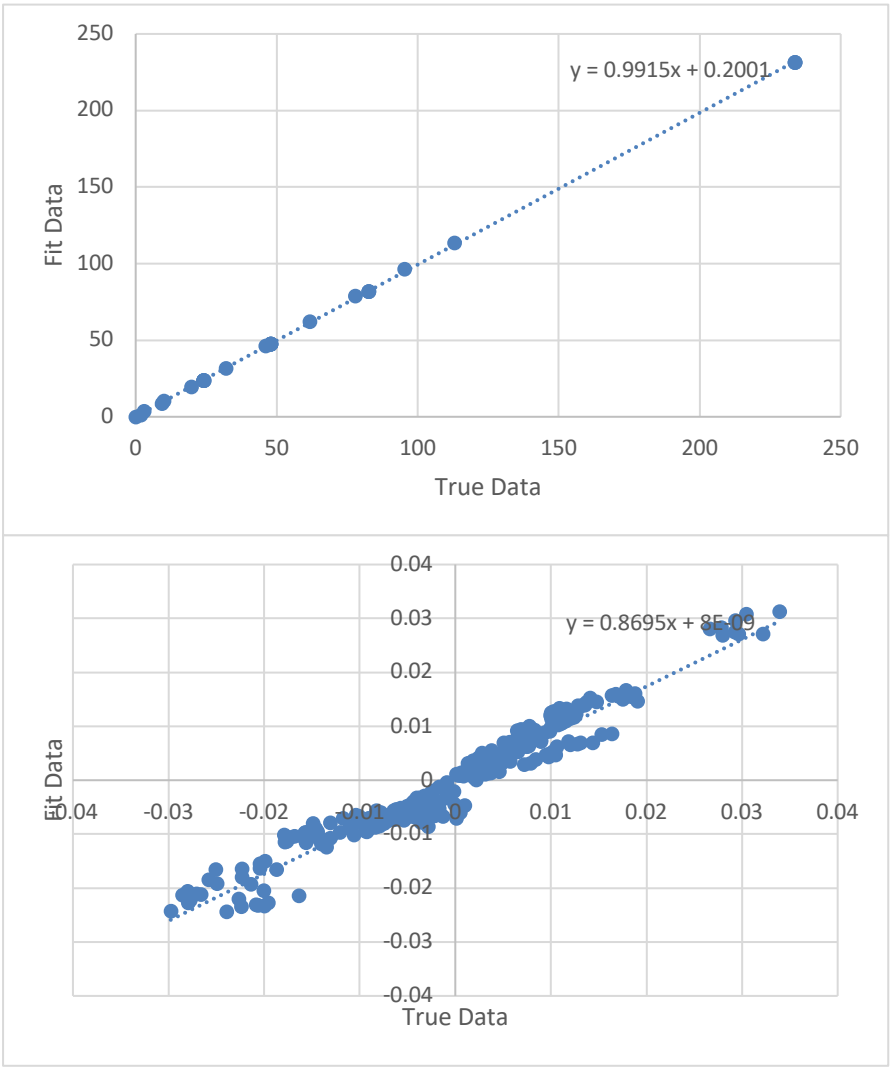

Figure 10. Comparison between ab-initio energy (up), force(down) vs MEAMfit produced EAM_Pot_1 Energy force

For the EAM_Pot_1 the energy seems to fit well though the force has a slope of .869 which tells it did not fit well. The reason for this bad fit might because of a large compression. The above force graph is for 0.92V structure of Ni3Al structure which had comparatively large

compression. This suggests that false sense of rigidity was produced by the volume reduction. This assumption seems correct when forces for no volume reduction structure was plotted and came with a slope near to 1.

Now we have plotted, in Figure 11, one of the best-produced EAM potentials which showed very encouraging results through thermal stability and mechanical properties, EAM_Pot_4. The optimization function for this fit was 0.24 which is very close to the suggested value (0.18) for MEAMfit fitting.

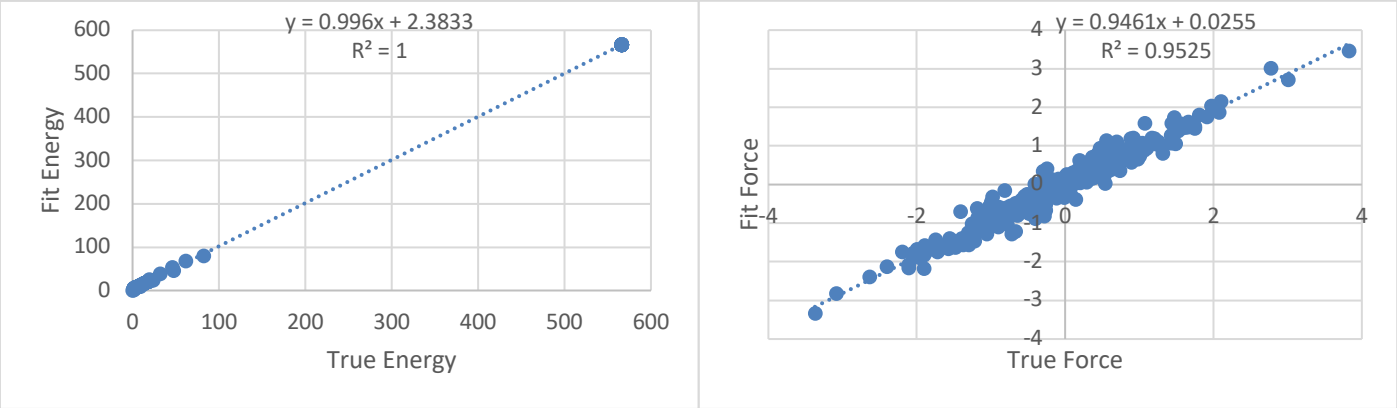

Figure 11. Comparison of Energy (left) and Force (right) of ab-initio data with EAM produced Data for EAM_Pot_4

The ab-initio Force and energy produce almost the same data for EAM produced Force and energy. The fitting potential is also evaluated as an individual potential, like pair potential, embedding energy and electron density in Figure 12. It seems the embedding functions are qualitatively matching with the common interpretations, like embedding energies, should decrease rapidly as the distance increases. But clearly, the plots fail to resemble the actual plots of Mishin. There could be many reasons behind these, Firstly in Mishin EAM potential, it has used several phases of Ni-Al structures. It's important for not being stuck in a reference structure and being over fitted for a particular structure.

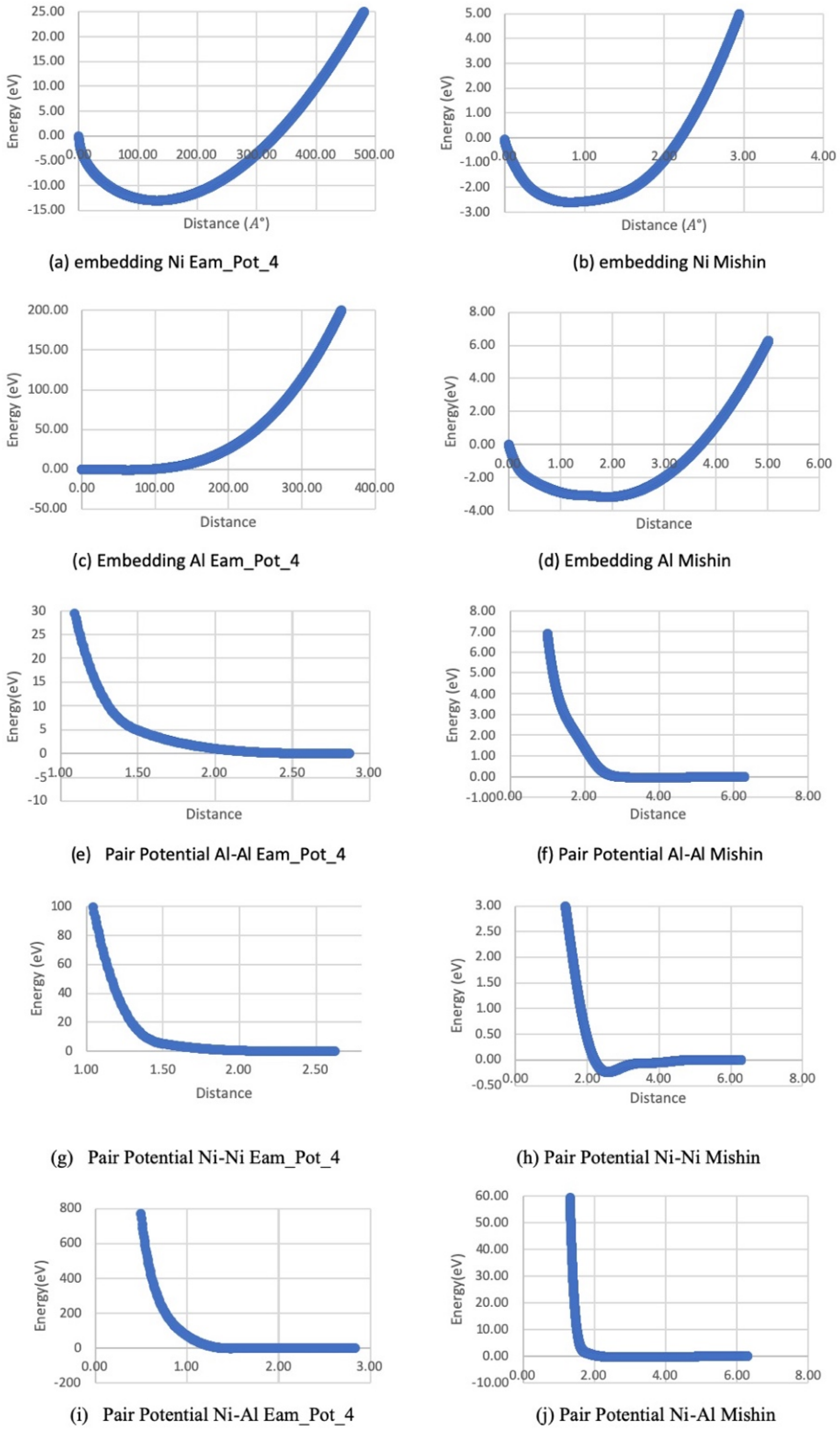

Figure 12. Comparison of the individual plots of the function between EAM_Pot_4 and Mishin

It happens when insufficient structural phases are used for inputs. Mishin for developing the NiAl potential used several phases of Ni-Al [52]: $L1_1(CuPt\ Prototype),\ B2,$ $B1(NaCl\ prototype), L1_0(CuAu\ prototype)$, "40" $(NbP\ prototype), D0_{22}, D0_3$. While in our case only $L1_1$ structures were used for developing EAM_Pot_4. Another reason could be the samples that we used has NPT samples mostly where the pressure was around zero KBar. In the NPT systems generally, the total force is very close to zero. And the different volume samples which have more pressure have very less number of trajectories, so that could not help giving enough energy. So for getting the dynamic range of energy information in the energy well we need to add more NVT sample with high pressure and high temperature.

DISCUSSIONS

After the fitting process, the created EAM potential was tested through several computational experiments for reliability. For the testing LAMMPS [26] code was used for performing the simulation. MEAMfit produces the LAMMPS readable format for EAM potential. Other than this MEAMfit also produce files that are used for visualization. The pair potential, embedding energy and electron density against the interatomic separation can be plotted through the files created by the MEAMfit.

These files were generated by running the MEAMfit again but putting NOOPT=true and POTFILEIN=filename (here the filename is the potparas_best1) in the setting file.
Now the first and vital analysis, that was done on the generated LAMMPS format EAM potential is the thermal stability check for Ni3Al structure at different temperatures. All of the crystalline structure generally exists in room temperature, so failing to reproduce that thermal stability will put a question to the optimized potential.

Ni3Al Thermal Stability and Mechanical Properties

For the thermal stability check, I created a supercell of $6 \times 6 \times 6$ supercell of the ordered FCC Ni3Al ($\gamma' prime$) structure. Later I ran NPT simulation through LAMMPS code. The atoms were given with semi-random initial velocities, the distribution was Gaussian. The ambient pressure was kept zero and relaxed volume was set. The reason for the relaxed volume is to catch the shape and volume change caused by the atoms only not by outside intervention. The NPT run gave a dump file that can be visualized in the OVITO software [45]. The script for thermal stability calculation is given in appendix.

In Figure 13, I am presenting a single frame from the NPT run. The atom's radius here was kept 0.5 $A°$.

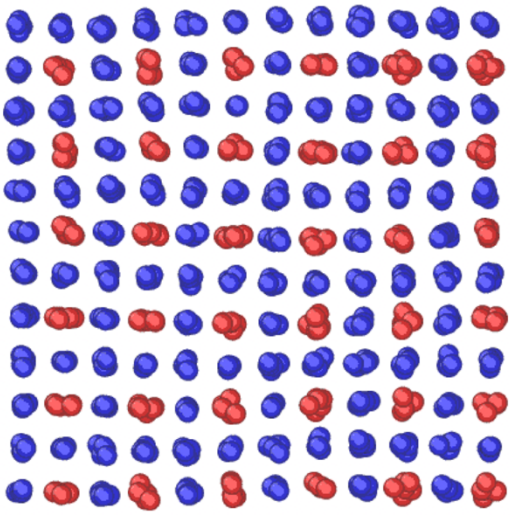

Figure 13. Thermal stability check for EAM-Pot_1 at 10K temperature.

Here in the EAM_Pot_1 is stable at 300K but it was expected to have less vibration which was a significant weak potential. We further checked the thermal stability at room temperatures and higher temperatures (Figure 14).

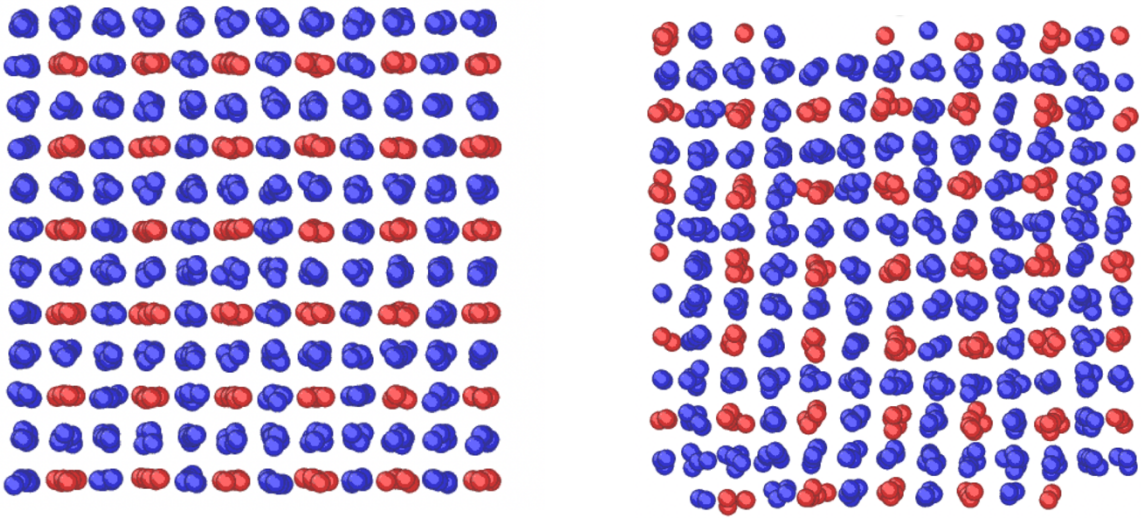

Figure 14. Thermal Stability check for EAM_Pot_1 300K and 1000K

I noticed more vibration in the structure of Ni3Al at room temperature which was clearly not the real representation of the thermal stability at these temperatures. The reason for this more vibration is because we have not trained the input data for higher temperatures. This mere thermal stability is coming from the different volumes ground state calculation which is giving this model a little range of different energy which helped it to be stable at 1000K with very bad vibration representation of the atoms. But this energy was not enough for replicating the higher temperature thermal stability at 1500K as we can see from Figure 15.

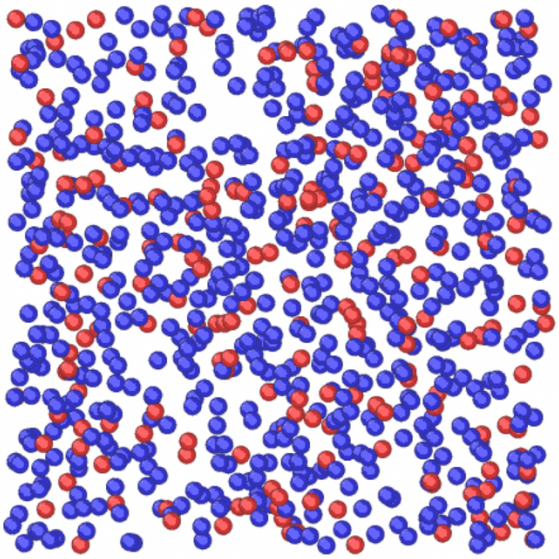

Figure 15. Thermal stability check for EAM_Pot_1 at 1500K

At 1500K the structure collapsed. The acquired data from the DFT was not enough for replicating the stability for higher temperature which tells to add different sets of input data here. But before adding different data it was needed to see whether the input data were fit properly. As mentioned earlier the NOOPT=true functions in MEAMfit give the fitting analysis. As we can see from Figure 16 the fitting of energy was almost perfect as the co-relation coefficient is .99. But still the force fitting was very bad. From a perfect fitting run, one could expect a trendline of

the comparison data would have 45^0 angle slope. This tells the reason why the stability was very poor in the discussed part.

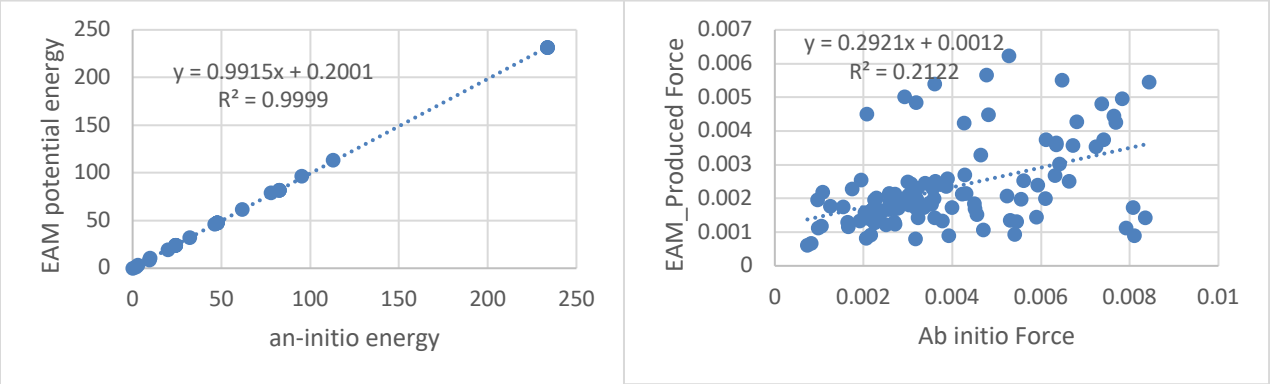

Figure 16. Comparison of energies from ab-initio data and MEAMfit produced EAM data. The dotted line showing the slope for the trendline.

EAM_Pot_2. As this EAM_Pot_1 failed in the analysis, we improved the model by adding different inputs that might help to stabilize the structure. For that, the next sets of inputs we put are one NPT samplings to the system. We put 300K NPT sampling to the force-fitting. The idea is to get the stabilization at a higher temperature, so I added the samplings for one NPT runs. I ran the MEAMfit exactly with the same settings as before. The next EAM potential that was created was EAM_Pot_2.

Then we checked the stability of that EAM_Pot_2 potential, in Figure 17 and Figure 18, at low temperature, room temperature, and higher temperature.

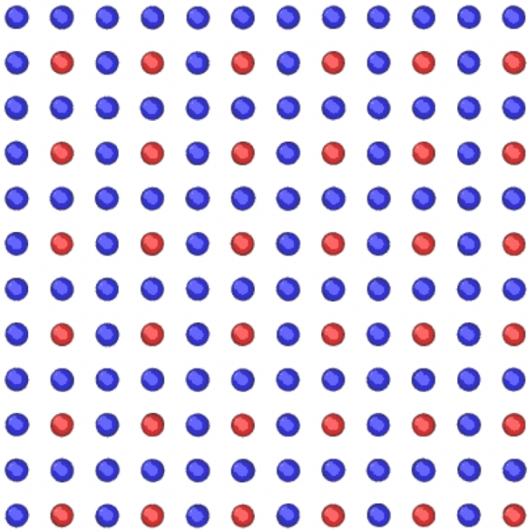

Figure 17. EAM_Pot_2 thermal stability at 10K

At low temperature, this EAM potential is more stable than the EAM potential 1. Atoms have very less vibration that is expected from this structure at low temperatures. Also, the atoms are fixated at its place which was not seen for the EAM_pot_1 at this temperature.

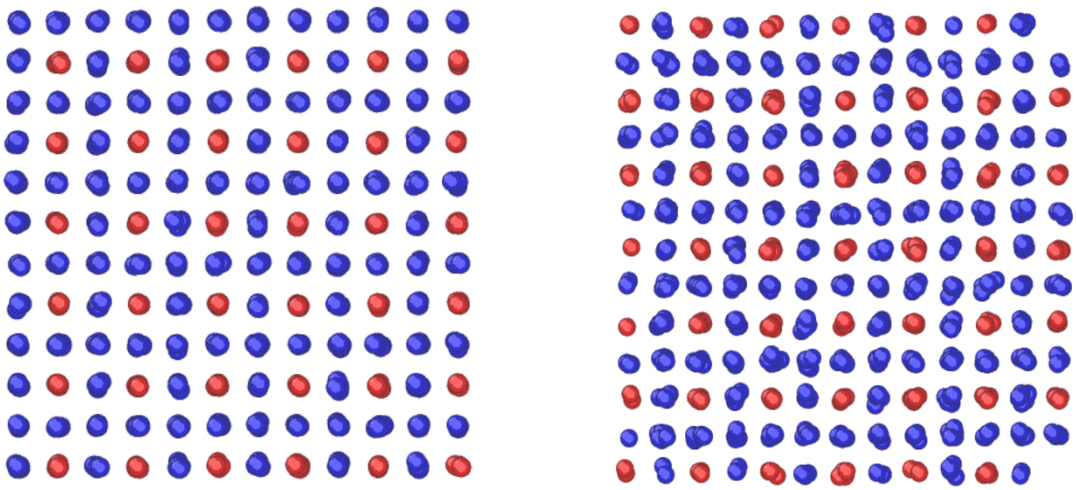

Figure 18. EAM_pot_2 thermal stability at 300K and 1000K

As we can see the thermal stability at room temperature and at higher temperature is visibly better than EAM_pot_1. It proves including the NPT samples improved the EAM potential in the thermal stability. And finally, we checked the thermal stability at 1500K in Figure 19. Though the inputs of this EAM_pot_2 did not have very high-temperature sampling it was found stable at 1500K.

At 1500K EAM_Pot_2 is stable and did not collapse as EAM_Pot_1. Which is a very good improvement. But the vibration of the atoms was still very fast. And I noticed some of the atoms were not fixated at its place. From this analysis, it was clear that these data were not

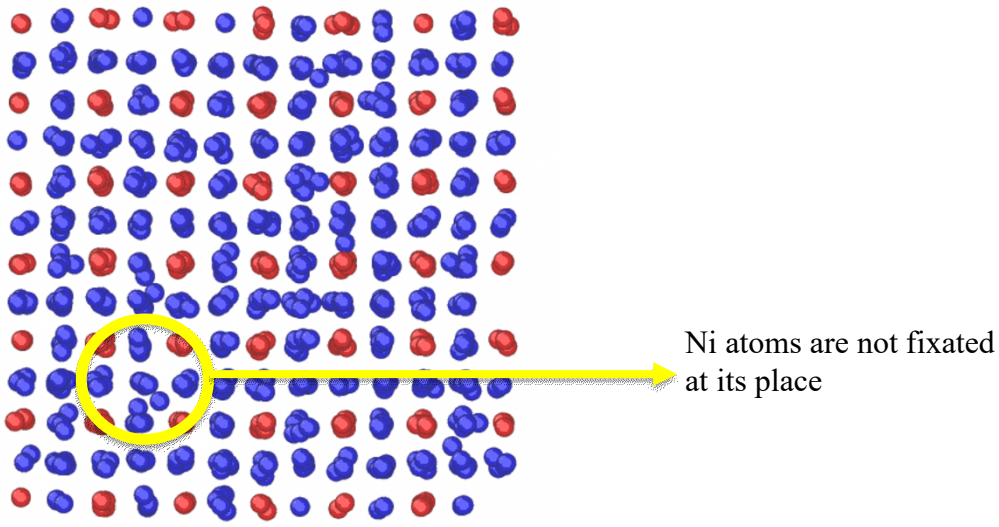

Figure 19. EAM_Pot_2 at 1500K

enough for getting a perfectly stable structure at the higher temperature. Then I added more NPT runs of higher temperatures in the system.

In Figure 20, I have compared the force-fitting for 700K and 1000K for EAM_Pot_2. For 700K the correlation coefficient is .34 and for 1000K it is .623 which tells the forces for this system did not fit well. This is definetly better then EAM_Pot_1 which had the co-relation

coefficient of .21 and that is why better stability at higher temperature was noticed. But still the force comparison was not satisfactory. That is why I added one more NPT file at 1500K.

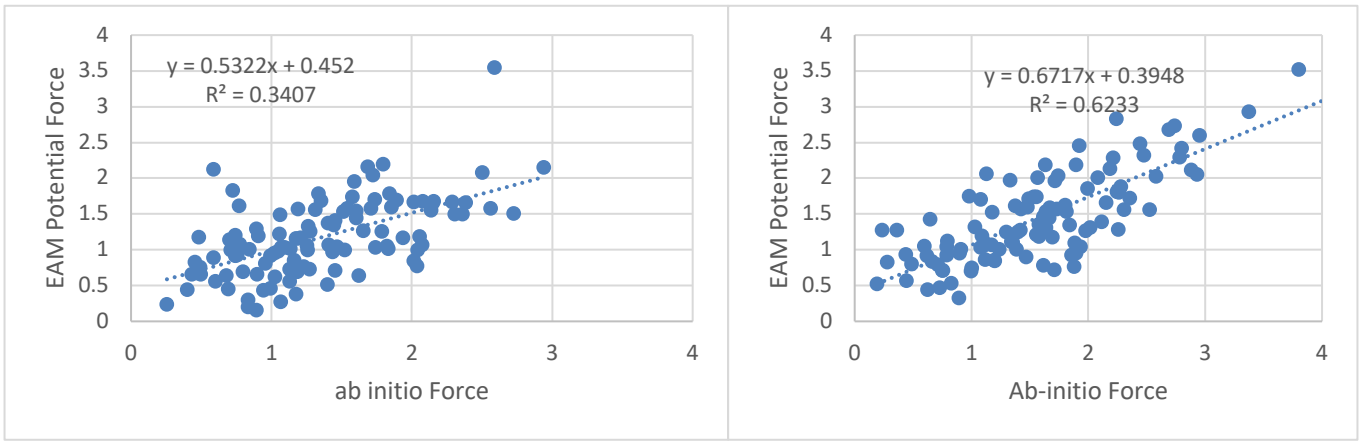

Figure 20. Comparison of resultant force at 700K and 1000K EAM_Pot_2 (true data vs fit data)

EAM_Pot_3. The next EAM potential was EAM_Pot_3 which has all 5 NPT runs at 300K, 500K, 1000K and 1500K. The idea of developing this potential was that adding more trained data for higher temperatures should stable structure with less vibration. The correlation coefficient is 0.6473 which represents a very bad fitting of forces is shown in Figure 21.

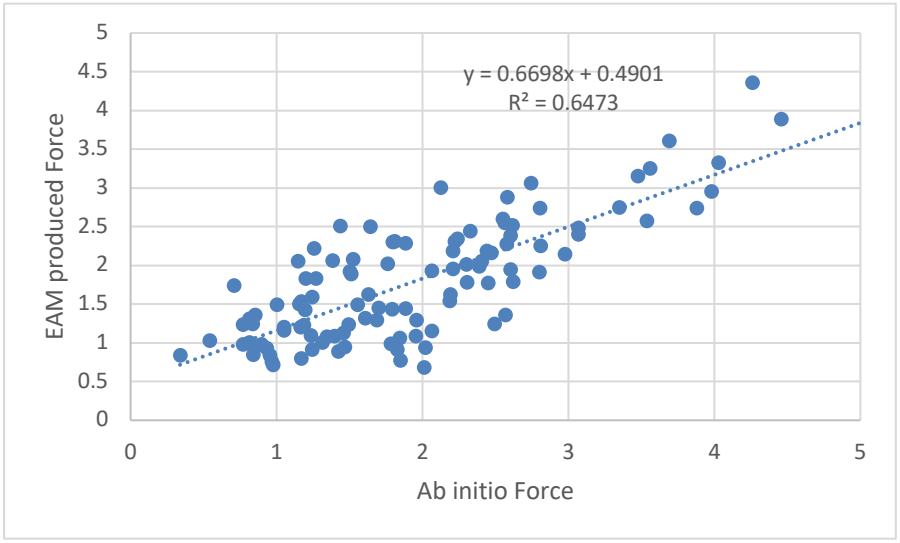

Figure 21. Comparison of resultant Force of EAM_Pot_3

Though the force-fitting was not very good but adding more NPT sampling to the system surely helped the thermal stability. Atoms are more fixated than before. In Figure 22, the thermal stability at different temperatures for EAM_Pot_3 was shown.

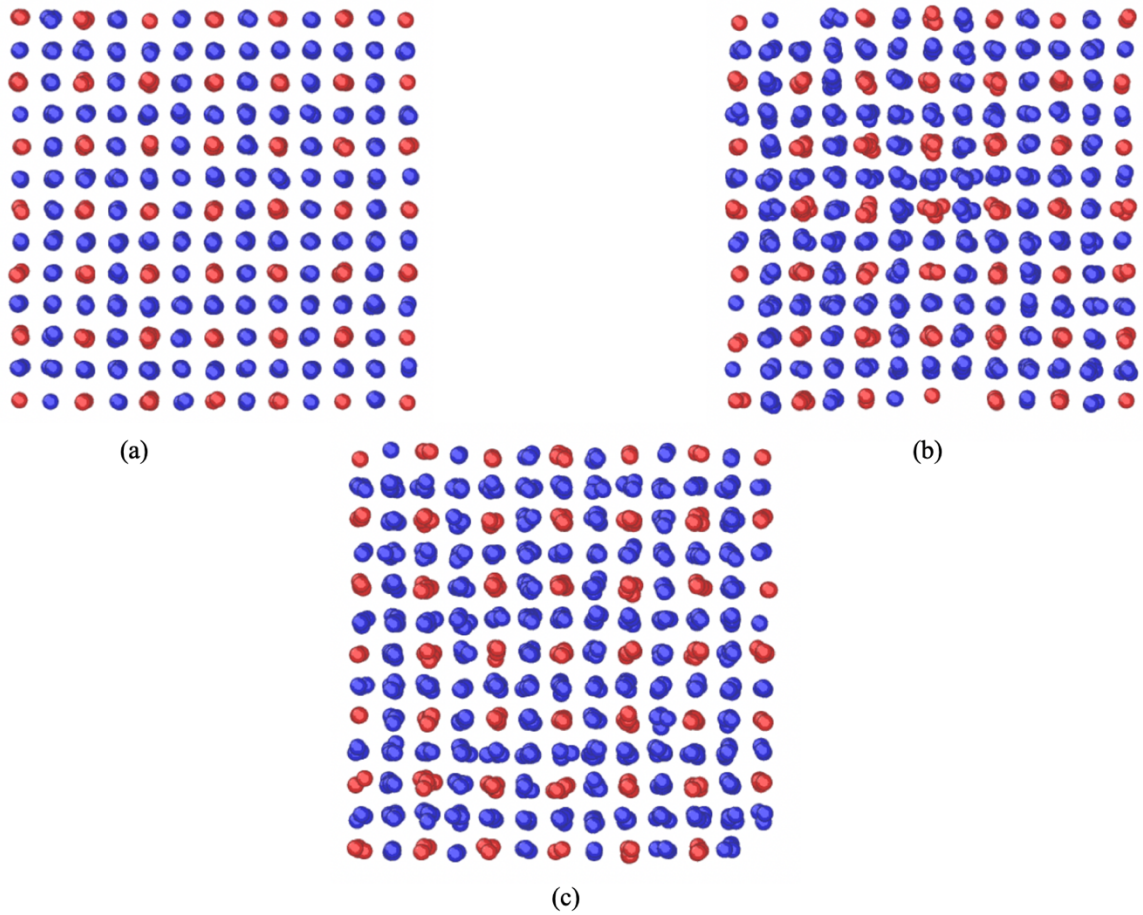

Figure 22. EAM_Pot_3 at (a) 300K, (b) 1000K and at (c)1500K.

As discussed before, after the thermal stability next analysis is the checking of the mechanical properties which is Elastic Constant. Elastic constants for an inorganic compound give the complete view of how that reacts with the external pressure provided the pressure is in the elastic limits. With elastic constants, one can have a fundamental insight of the nature of the bonding between the atoms. The script for elastic constant calculation can be found in appendix.

Here in Table 3, I compared the elastic constants of my generated EAM potential with two sets of reference values. One with the EAM potential created by Mishin[53] and another with the experimental values for Ni3Al [54].

Table 3. Comparison of Elastic Constants of developed EAM potentials.

	EAM_Pot_1 (GPa)	EAM_Pot_2 (GPa)	EAM_Pot_3 (GPa)	Mishin_EAM_pot (GPa)	Experimental (GPa)
Bulk Modulus	201.92	505.51	505.994	184.04	173.83
Shear Modulus-2	48.78	50.37	25.70	45.74	37.85
Shear Modulus-1	80.32	93.12	93.40	125.84	125.8
Poisson Ratio	0.388	0.451	0.475	0.3852	0.40

Here I noticed the bulk, shear modulus-1, and shear modulus-2 were far off the reference values overall. Though interesting facts were seen in EAM_Pot_1 which showed previously very bad representation in the thermal stability has a bulk modulus close to the reference values. The reason behind this is because Bulk modulus is the relation between the uniform and perpendicular pressure with the volume of the system.

And EAM_Pot_1 had the sampling of different volumes structures. And in one way these sampling captures the movements of the atoms which can represent the bulk modulus properties. That is why EAM_Pot_1 has a better bulk modulus. A visual representation is given in Figure 23

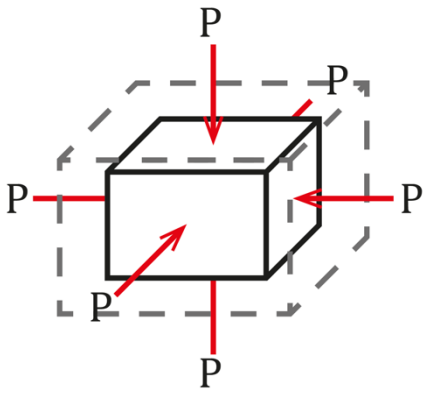

Figure 23. Illustration of uniform compression

But for shear modulus it needs some of the axis movements which EAM_Pot_1 lack. But EAM_Pot_2 and EAM_Pot_3 have NPT samplings which helped to get the shear modulus to get a little closer than the EAM_Pot_1. To understand this deeply we compared the individual constants C11, C12, and C44 also of all of these potentials in Table 4. The C11 for EAM_Pot_1 is very close to the reference values but none of the other parameters is close.

Table 4. Comparison of Cij of all the developed EAM with Mishin and experimental values

	EAM_Pot_1 (GPa)	EAM_Pot_2 (GPa)	EAM_Pot_3 (GPa)	Mishin_EAM_Pot (GPa)	Experimental (GPa)
C11	252.452	572.67	540.26	245.038	224.3
C12	190.88	471.92	488.85	153.54	148.6
C44	84.18	93.12	93.5	125.84	125.8

EAM_Pot_4. From the above two charts it was concluded none of these EAM potentials has proper elastic constants. So, in the next EAM potential, I added all the ground state samplings and all the NPT runs hoping that both sets of data would improve the bulk and shear modulus. In Table 5, I have compared the elastic constants of EAM_Pot_4 with the reference values.

Table 5. Comparison of Elastic Constants of EAM_Pot_4 with experimental values

	EAM_Pot_4 (GPa)	Mishin_EAM_Pot (GPa)	Experimental (GPa)
Bulk Modulus	171.225	184.04	173.83
Shear Modulus-2	26.61	45.78	37.85
Shear Modulus-1	78.86	125.84	125.8
Poisson ratio	.42	0.3852	0.40
C11	206.715	245.03	224.3
C12	153.48	153.54	148.6
C44	78.86	125.84	125.8

As we can see the Elastic Constants improved largely with the mixing of all the different volumes ground state sampling and 5 different NPT samplings. Bulk modulus is 15.63% off from the Mishin_EAM_Pot's Bulk modulus, shear-2 is 41.87% off where shear-1 is 37.33% off. Also, C12 is almost the same. We know, with increasing temperatures elastic constant values get decreased [55]. That is why all the elastic constant calculation was done in room temperature here. Figure 24 shows the resultant ab-intio vs EAM produced force comparison of EAM_Pot_4.

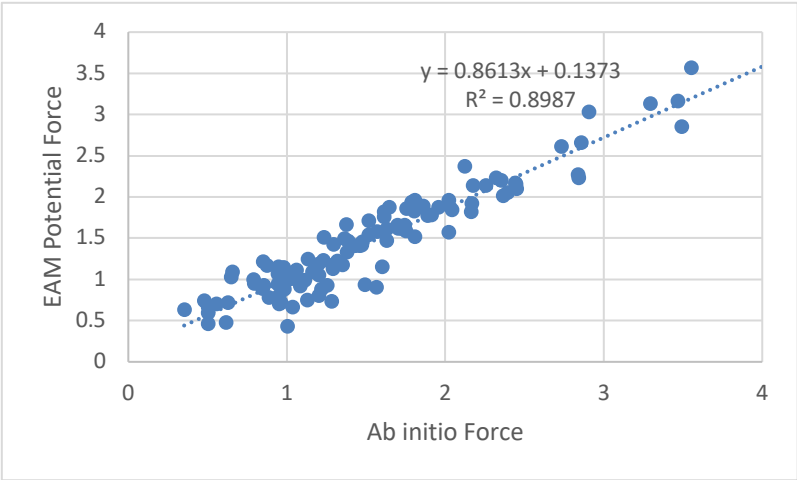

Figure 24. Comparison of Force EAM_Pot_4 (true data vs fit data)

The force-fit better than the previous models as the correlation coefficient is 0.897. For getting more into the deep behind this mismatches in the elastic constants I plotted the resultant stress of true data vs fit data of EAM_Pot_4 (Figure 25).

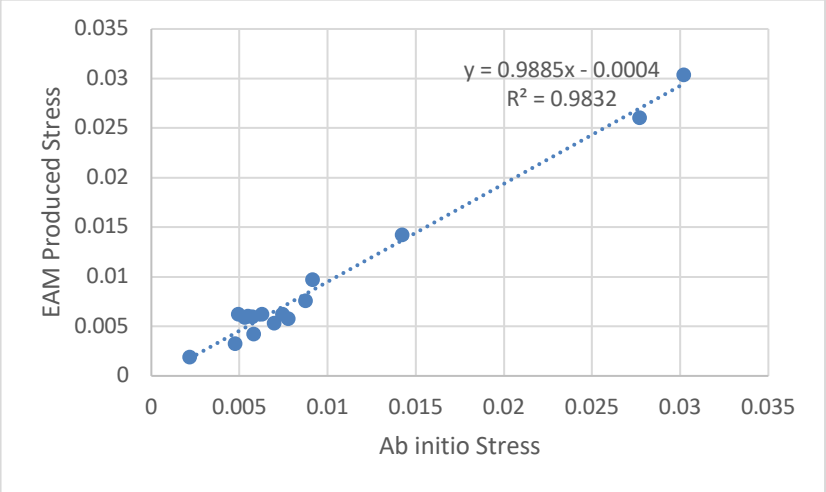

Figure 25. Comparison of the stress of EAM_Pot_4 (fit data vs true data)

The correlation coefficient of Figure 25 is 0.98 which suggests the fit for stress was almost

perfect. So the input data was lacking the correct elastic constants that were the reason the EAM_Pot_4 did not have correct Cij samples.

EAM_Pot_5. Still, there was a large place for improvement and these samplings were not enough. So, a different set of data was needed. Then Cij samplings that I generated through VASP were included in the EAM_Pot_4 system which gave EAM_Pot_5. This Cij sample which had 37 trajectories all were included in the MEAMfit run. I compared the elastic constant of EAM_Pot_5 in Table 6.

Table 6. Comparison of Elastic Constants of EAM_Pot_5

	EAM_Pot_5 (GPa)	Mishin_EAM_Pot (GPa)	Experimental (GPa)
Bulk Modulus	204.76	184.04	173.83
Shear Modulus-2	41.28	45.78	37.85
Shear Modulus-1	101.08	125.84	125.8
Poisson ratio	0.40	0.3852	0.40
C11	259.81	245.03	224.3
C12	177.23	153.54	148.6
C44	101.08	125.84	125.8

In EAM_Pot_5 Elastic Constants were improved far more with the included with the Cij samples than any other previous models. The Bulk modulus 11% off, Shear Modulus-2 was 8.8% off, Shear Modulus-1 was 19.2% off, Poisson ratio 5% off, C11 was 5.7% C12 was 15.8% off from the Mishin's EAM potential. And also from the stress comparison of Figure 26, it can be seen how well the stress information fit for ab intio data.

But this time another thing is needed to check is whether this added Cij sampling did any damage to thermal stability. So, the thermal stability at 1500K was checked in Figure 27.

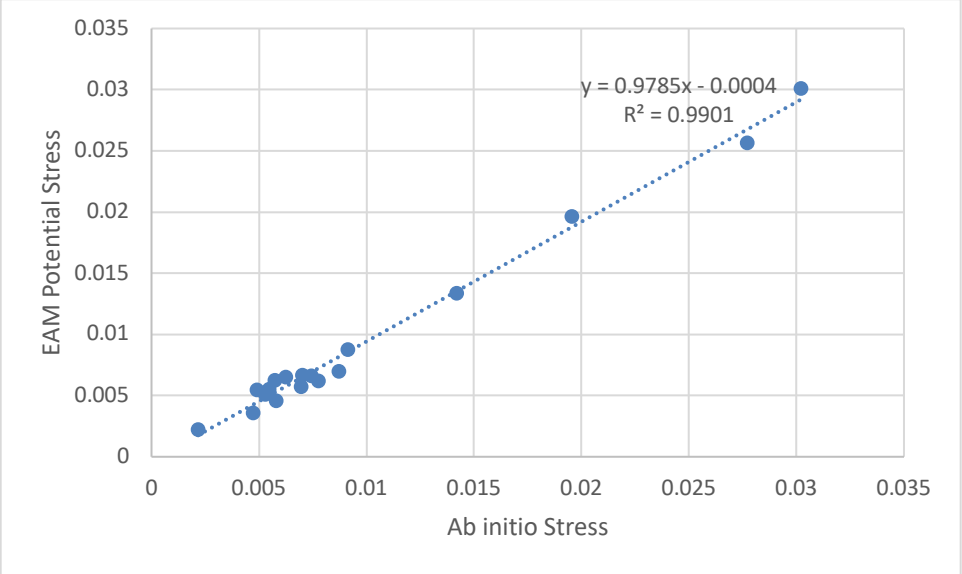

Figure 26. Comparison of resultant Stress of EAM_Pot_5 (true data vs fit data)

Here at 1500K the EAM_Pot_5 was found stable though Ni atoms vibration was more noticeable than the previous model. Further, in Figure 28 I compared the resultant force of ab-intio data with EAM produced data. The correlation coefficient is 0.905 which is so far the most

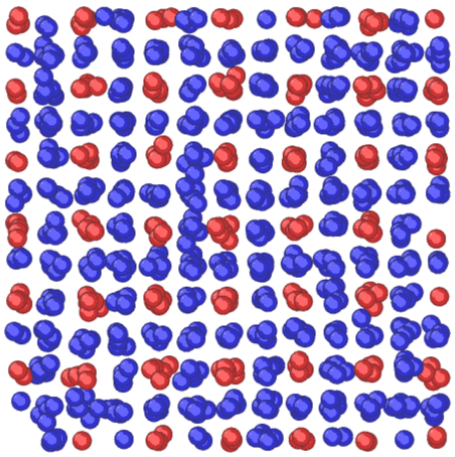

Figure 27. The thermal stability of EAM_Pot_5 at 1500K

accurate than any previous model. This force-fit comparison and stress comparison is very congruent with the thermal stability and mechanical properties result.

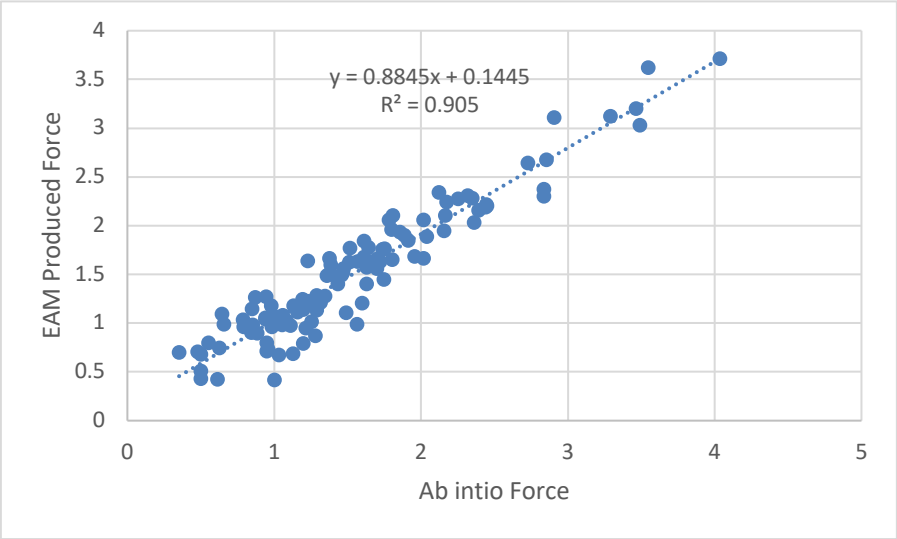

Figure 28.Comparison of Force of EAM_Pot_5 (true data vs fit data)

Transferability. One important analysis is transferability. One good EAM potential should be stable on different structures of Ni-Al. So, the optimized EAM potentials were also tested to assess the thermal stability of other crystal structures or phases aside from the original phase. I checked the thermal stability (Figure 29) of the developed EAM potentials on the

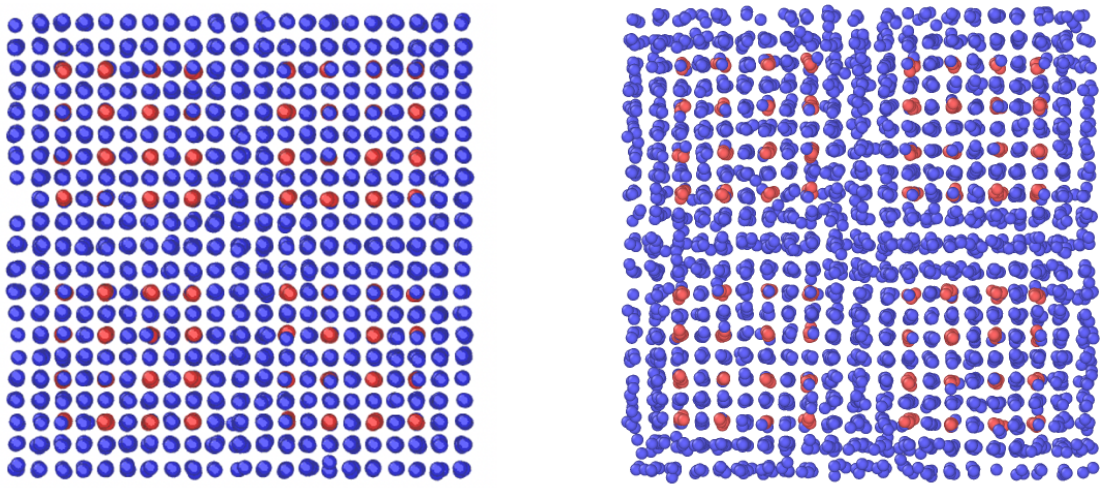

Figure 29. Gamma Gamma Prime thermal stability for EAM_Pot_5 at 300K (a) and at 1000K (b).

Gamma_Gamma_prime ($\gamma\gamma'$) phase at room temperature and also at high temperature. The EAM_Pot_4 failed at thermal stability even at room temperature but EAM_Pot_5 which has a C_ij sample was stable at room temperature. Though unphysical vibrations were noticed at high temperatures. One thing was to notice is that the Ni atoms were having more vibrations than the Al atoms. But one should expect Ni atoms to be less vibrated as this heavier than Aluminum. One reason can be that all the input samples were used the fcc structure of Ni3Al. There were not enough data that could show the bonding between just for Pure Ni. But in Table 7, I compared the elastic constants of pure Ni and found its very close to the experimental values.

Table 7. Elastic Constant of Pure Ni of EAM_Pot_5

	EAM_Pot_5 (GPa)	Mishin_EAM_Pot (GPa)	Materials_Project (GPa)
Bulk Modulus	213.17	206.83	198
Shear Modulus-2	44.98	43.479	58
Shear Modulus-1	121.01	140.06	132
Poisson ratio	0.40	.40	0.381
C11	273.15	264.80	276
C12	183.18	177.84	159
C44	121.01	140.06	132

EAM_Pot_6. Then, I introduced another phase to our model and that is the slab structure. In the slab structure, the middle part contains the Gamma prime structure while the two tails have a gamma phase which is pure Ni part. In the same way before, NPT runs at different

temperatures of this structure were included and EAM_Pot_6 was developed. The EAM_Pot_6 was more stable at high temperatures. In Figure 30, both at room temperature and high temperature the gamma-gamma prime structures are shown.

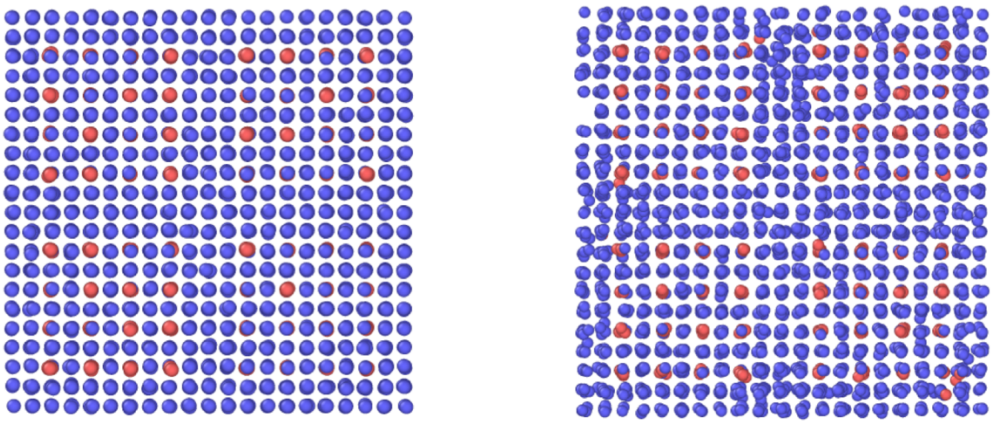

Figure 30. Gamma Gamma Prime stability for EAM_Pot_6 at 300K (a) and at 1000K (b).

But as a trade-off, I had to lose the other mechanical properties like Elastic Constants for Ni3Al. This left another place to work on of while improving the structure thermal stability at different temperatures for different phases, the mechanical properties should be also be kept intact. In Figure 31, I compared the forces generates from the slab sample at 1500K.

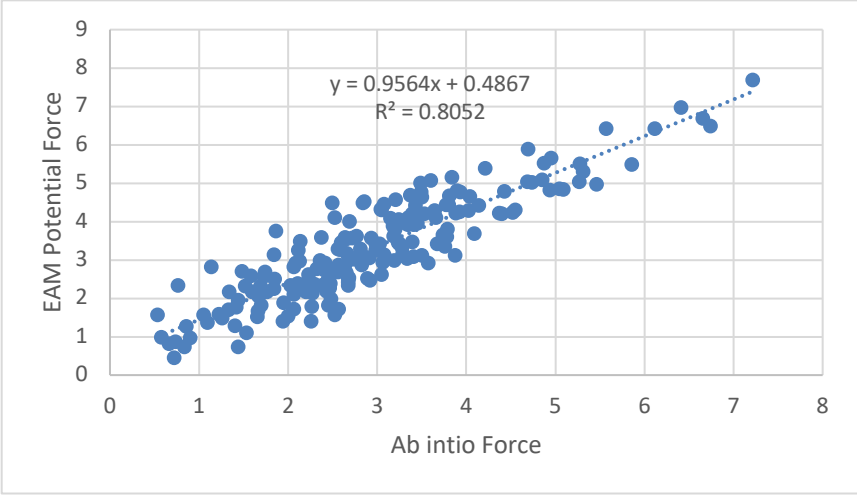

Figure 31. Comparson of resultant force on slab strucutre at 1500K

As it's clear from here adding high temperatures sampling for particular this structure (slab) fit very well. This indicates the reason behind the thermal stability at higher temperature. And these new slab structures also affected the other samples in the fitting process. I checked the force-fitting for the Ni3Al sample. In the previous model EAM_Pot_5, the thermal stability at 1500K was well enough but we noticed more vibration in the EAM_Pot_5 model comparive to the EAM_Pot_4. But adding the slab structure not only helped the thermal stability for gamma-gamma-prime structure but also in the Ni3Al structure as we can see from Figure 32.

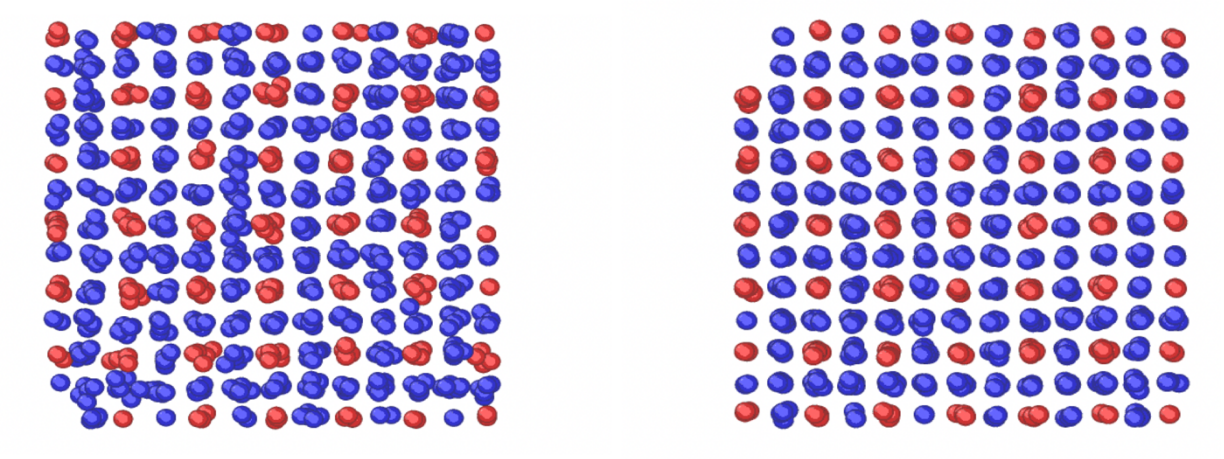

Figure 32.Thermal stability of EAM_Pot_5 (left) and EAM_Pot_6 (right) at 1500K

Carbides Thermal Stability

With the same approach described three different EAM potentials were developed for Carbides Phases. $Mo_{23}C_6$, $W_{23}C_6$ *and* $Cr_{23}C_6$ and also, their thermal stability was checked at room temperature and at a higher temperature. In general carbide systems have very high melting point than Ni3Al structure. So for thermal stability one had to add very high temperature sampling to the fitting process. For creating the samples we went till 3000K NPT and NVT run. $Cr_{23}C_6$ had the training data of high-temperature NPT samples till 2000K with one relaxed volume structure.

For thermal stability check, a supercell was created, and the atoms were given semi-random initial velocity with keeping ambient pressure zero. Then for the developed EAM potential, MD simulation was performed on this structure. Figure 33 shows, the generated EAM potential is stable at room temperature and at 1500K with force comparison having correlation coefficient 0.97. Also, the transferability of this EAM_Pot was checked for different phases at different temperauteres.

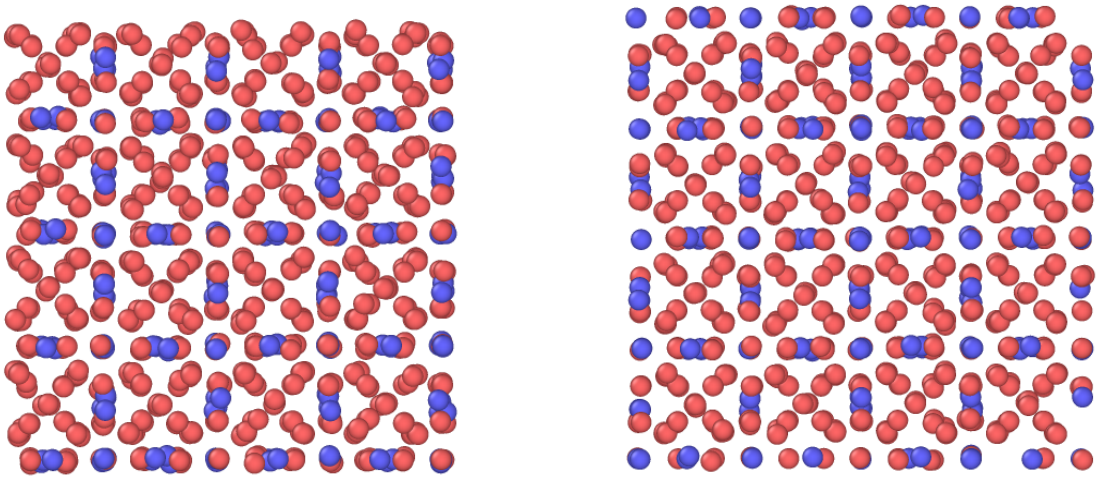

Figure 33. Thermal Stability of $Cr_{23}C_6$ at 300K and 1500K

And in Figure 34, I compared the fit force vs true force which shows a well fit.

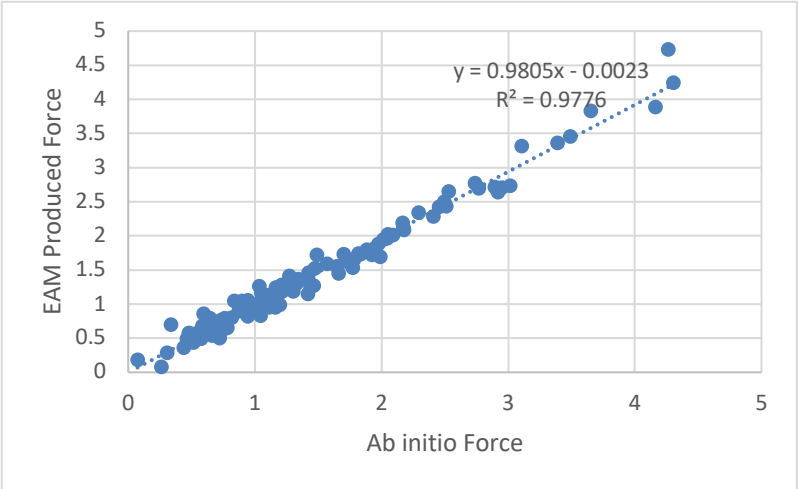

Figure 34. Force Comparison of $Cr_{23}C_6$ (true data vs fit data)

this EAM potential was checked for different phases of CrC at different temperatures Figure 35. Different phases of $Cr_{23}C_6$ were, CrC, pure Cr and Cr_3C_2. All of the structures were stable with realistic vibration.

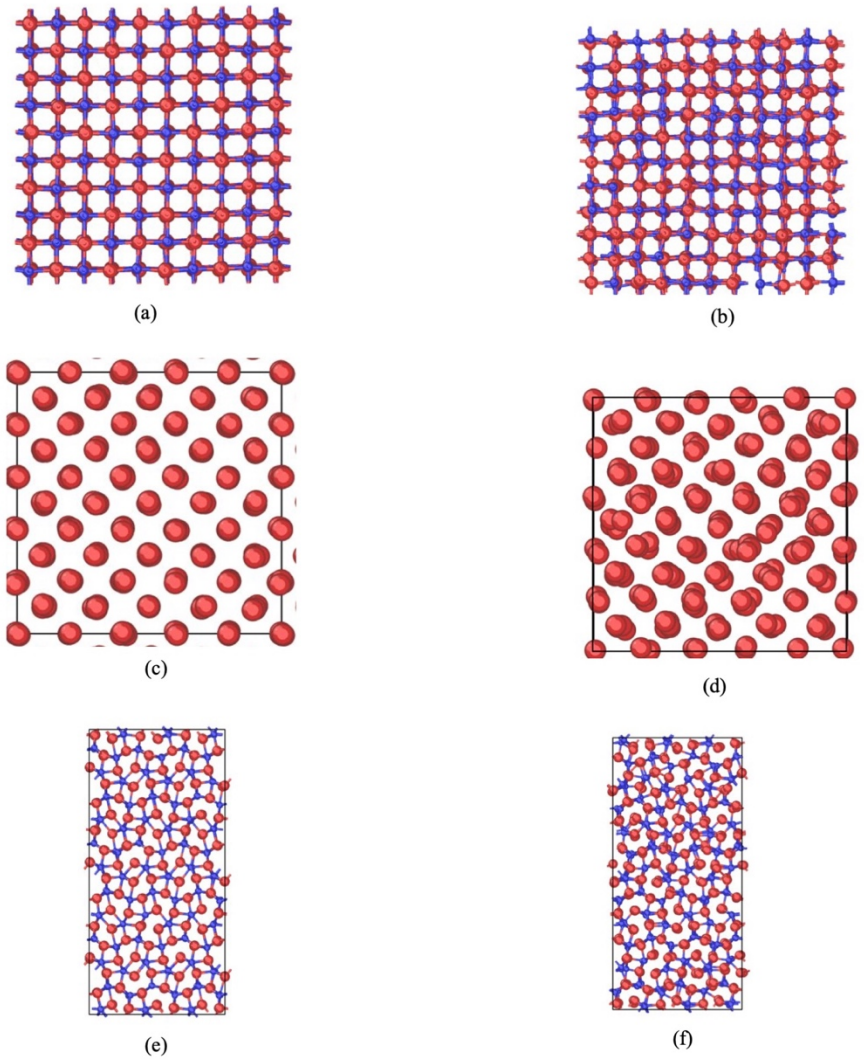

Figure 35. tranferability of $Cr_{23}C_6$ at 300K and 1500K in different structure (a) CrC at 300K (b) CrC at 1500K (c) Cr at 300K (d) Cr at 1500K (e) Cr_3C_2 at 300K (f) Cr_3C_2 at 1500K

$\boldsymbol{W_{23}C_6}$. The developed EAM potential for $W_{23}C_6$ was also found stable at room temperature and also at high temperature. In Figure 36 the thermal stability at two different

temperatures is shown. In developing this potential, we used only NVT samples of at 2000K, 3000K, containing almost 700 trajectories. NVT samples each had pressure around 1800Kbar. Apparently, this pressure caused more energy to the system than a NPT system can do. In the NPT system though atoms experience different forces it's the total energy is close to zero. On the other hand, NVT samples with constant pressure have more energy than the NPT system. This is why NVT systems had better effects than NPT.

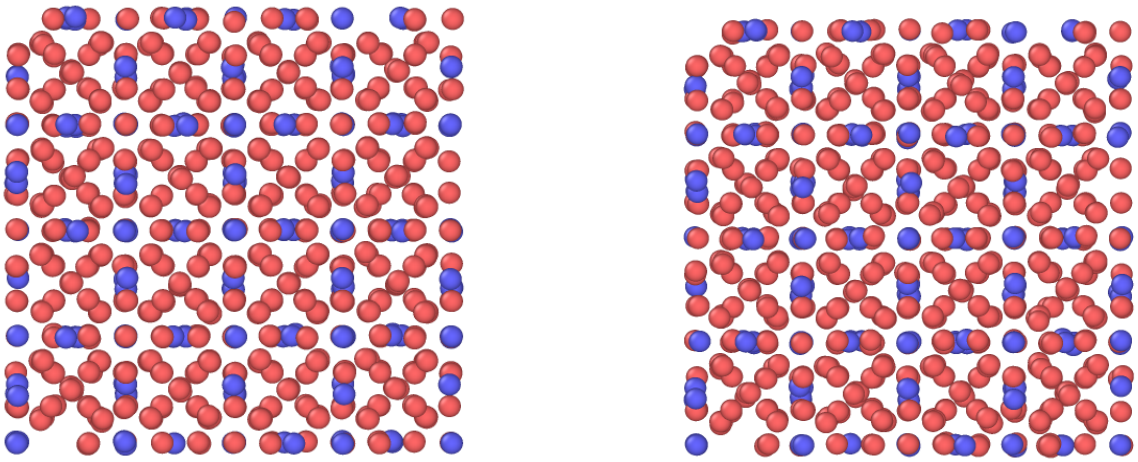

Figure 36. Stability of $W_{23}C_6$ at room temperatures and 1500K

So far, in these models we have only used the NPT and NVT samples for the thermal stability. Getting the Cij property from carbide structure is bit hard than the previously discussed crystal structure of Ni3Al. But in our next approach that's what we are aiming for, feeding the the Cij samples to the fitting process to these carbides systems.

CONCLUSION

In this chapter, I will summarize the conclusion of this study, also will review the effectiveness of MEAMfit. I will talk about some of the shortcomings in our process. And lastly, I will talk more about the future steps that should be done for creating more robust EAM potential.

The goal of this project is to develop a potential for Ni-based superalloy through the force-fitting method. The processes that were followed, are creating the appropriate structures and then performing AIMD calculation for getting force and energy data for a specific system and then fitting those trained data to a particular potential function to develop the desired potential.

All the discussions I presented in the last chapter showed us how MEAMfit is giving us consistent results with the input data. It fitted the trained data to the given EAM potential function and produced the EAM potential that successfully gave the expected results. The first priority from the EAM potential was to get the thermal stability at a higher temperature which with the high NPT trained data we were able to get. The structures were found stable even at 1500K with realistic vibration. The next priority was to get mechanical property. By using Cij we achieved elastic constants value that is close to experimental values. The deeper analysis of force, the energy, stress error of ab-initio data with EAM developed data gave us the idea of how MEAMfit was fitting with the given input and also gave us indication for the next set of inputs. Unlike any other force-fitting code like POTFIT, this code has very user-friendly, with minimal input.

Our approach towards training the potential step by step also seems effective. The system lacking NPT samples failed at thermal stability at a higher temperature. And high NPT

samplings solved that problem. Different NPT samples at high temperatures stabled the structure at 1500K. The EAM_Pot_5 was found stable and the mechanical properties (elastic constants) were also close to the accurate. But the structure was lacking the properties of transferability. Adding another phase (gamma-gamma prime slab) of the structure made it thermally stable in gamma-gamma-prime phase. Though in the newest model, more NPT samples were used comparative to Cij sample which made it mechanically unstable. But fortunately MEAMfit provides way to give comparative weight to the fitting property and that is what our next approach to get around this problem.

We also found that NPT and NVT inputs had better impacts than the different volumes of relaxed samplings. The thermal stability for both Ni3Al and carbides phases NVT and NPT samplings with enough number of trajectories stabled our structures.

One issue with the total process was, it took a long time for fitting the force and energy. MEAMfit software, can only do serial jobs which takes comparatively more time for softwares which can do the parallel jobs. Currently the developer of this code trying to improve the code for making it run in the parallel.

In the future, I will be adding different phases of Ni3Al instead of just gamma-gamma prime for achieving more transferable properties. Next step would be adding more elements to the system for getting superalloy's EAM potential. And for the carbides, Cij samples will be added for getting the mechanical properties.

REFERENCE

[1] D. Furrer and H. Fecht, "Ni-based superalloys for turbine discs," *JOM*, vol. 51, no. 1, pp. 14–17, 1999.

[2] P. Caron and T. Khan, "Evolution of Ni-based superalloys for single crystal gas turbine blade applications," *Aerosp. Sci. Technol.*, vol. 3, no. 8, pp. 513–523, 1999.

[3] C. T. Sims, N. S. Stoloff, and W. C. Hagel, *superalloys II*. Wiley New York, 1987.

[4] G. L. Erickson, "A new, third-generation, single-crystal, casting superalloy," *JOM*, vol. 47, no. 4, pp. 36–39, 1995.

[5] R. Dreshfield and R. Ashbrook, "Effects of sigma-phase formation on some mechical properties of wrought nickel-base superalloys," *Nasa*, vol. 100, no. May 1974, 1974.

[6] G. L. Erickson, "The development of the CMSX-11B and CMSX-11C alloys for industrial gas turbine application," in *Eighth International Symposium on Superalloys (Superalloys 1996), Champion, PA, Sept*, 1996, pp. 22–26.

[7] W. S. Walston, K. S. O'hara, E. W. Ross, T. M. Pollock, and W. H. Murphy, "RENfi N6: THIRD GENERATION SINGLE CRYSTAL SUPERALLOY."

[8] G. L. Erickson, "The development and application of CMSX-10," *Superalloys 1996*, pp. 35–44, 1996.

[9] T. M. Pollock and S. Tin, "Nickel-based superalloys for advanced turbine engines: Chemistry, microstructure, and properties," *J. Propuls. Power*, vol. 22, no. 2, pp. 361–374, 2006.

[10] M. Durand-Charre, "The Microstructure of Superalloys, Gordon and Breach." Amsterdam, 1997.

[11] E. S. Huron, "Serrated yielding in a nickel-base superalloy," *Superalloys 1992*. TMS-AIME, pp. 675–684, 1992.

[12] T. M. Pollock and R. D. Field, "Dislocations and high-temperature plastic deformation of superalloy single crystals," in *Dislocations in solids*, vol. 11, Elsevier, 2002, pp. 547–618.

[13] E. A. Loria, “Superalloy 718: Metallurgy and applications; Proceedings of the International Symposium, Pittsburgh, PA, June 12-14, 1989,” Warrendale, PA (US); Minerals, Metals and Materials Society, 1989.

[14] N. Saunders, A. P. Miodownik, and J. P. Schillé, “Modelling of the thermo-physical and physical properties for solidification of Ni-based superalloys,” *J. Mater. Sci.*, vol. 39, no. 24, pp. 7237–7243, 2004.

[15] A. Mottura, R. T. Wu, M. W. Finnis, and R. C. Reed, “A critique of rhenium clustering in Ni-Re alloys using extended X-ray absorption spectroscopy,” *Acta Mater.*, vol. 56, no. 11, pp. 2669–2675, 2008.

[16] P. Hohenberg and W. Kohn, “Physical Review 136,” *B864*, 1964.

[17] N. D. Mermin, “Thermal properties of the inhomogeneous electron gas,” *Phys. Rev.*, vol. 137, no. 5A, p. A1441, 1965.

[18] W. Kohn and L. J. Sham, “Self-consistent equations including exchange and correlation effects,” *Phys. Rev.*, vol. 140, no. 4A, p. A1133, 1965.

[19] G. Kresse and J. Furthmüller, “Software VASP, vienna (1999),” *Phys. Rev. B*, vol. 54, no. 11, p. 169, 1996.

[20] R. Zhou, *Molecular modeling at the atomic scale: Methods and applications in quantitative biology*. CRC Press, 2014.

[21] B. J. Alder and T. E. Wainwright, “Phase transition for a hard sphere system,” *J. Chem. Phys.*, vol. 27, no. 5, pp. 1208–1209, 1957.

[22] A. Rahman, “Correlations in the motion of atoms in liquid argon,” *Phys. Rev.*, vol. 136, no. 2A, p. A405, 1964.

[23] H. C. Andersen, “Molecular dynamics simulations at constant pressure and/or temperature,” *J. Chem. Phys.*, vol. 72, no. 4, pp. 2384–2393, 1980.

[24] D. J. Evans and B. L. Holian, “The nose–hoover thermostat,” *J. Chem. Phys.*, vol. 83, no. 8, pp. 4069–4074, 1985.

[25] J. Stadler, R. Mikulla, and H.-R. Trebin, “IMD: a software package for molecular dynamics studies on parallel computers,” *Int. J. Mod. Phys. C*, vol. 8, no. 05, pp. 1131–1140, 1997.

[26] S. Plimpton, “Fast parallel algorithms for short-range molecular dynamics,” *J. Comput.*

Phys., vol. 117, no. 1, pp. 1–19, 1995.

[27] W. D. Wilson, C. L. Bisson, and M. I. Baskes, "Self-trapping of helium in metals," *Phys. Rev. B*, vol. 24, no. 10, p. 5616, 1981.

[28] M. S. Daw and M. I. Baskes, "Application of the embedded atom method to hydrogen embrittlement," in *Chemistry and physics of fracture*, Springer, 1987, pp. 196–218.

[29] M. Mihalkovič and C. L. Henley, "Empirical oscillating potentials for alloys from ab initio fits and the prediction of quasicrystal-related structures in the Al-Cu-Sc system," *Phys. Rev. B*, vol. 85, no. 9, p. 92102, 2012.

[30] M. S. Daw, S. M. Foiles, and M. I. Baskes, "The embedded-atom method: a review of theory and applications," *Mater. Sci. Reports*, vol. 9, no. 7–8, pp. 251–310, 1993.

[31] Y. Mishin, M. J. Mehl, and D. A. Papaconstantopoulos, "Phase stability in the Fe–Ni system: Investigation by first-principles calculations and atomistic simulations," *Acta Mater.*, vol. 53, no. 15, pp. 4029–4041, 2005.

[32] J. Tersoff, "Modeling solid-state chemistry: Interatomic potentials for multicomponent systems," *Phys. Rev. B*, vol. 39, no. 8, p. 5566, 1989.

[33] M. Müller, P. Erhart, and K. Albe, "Analytic bond-order potential for bcc and fcc iron—comparison with established embedded-atom method potentials," *J. Phys. Condens. Matter*, vol. 19, no. 32, p. 326220, 2007.

[34] P. Paufler, "JH Westbrook, RL Fleischer (eds.). Intermetallic Compounds. Principles and Practice. John Wiley & Sons, Chichester 1995. Vol. 1. Principles. 1126 S. ISBN 0–471–94219–7. Vol. 2: Practice. 752 S. ISBN 0–471–93454–2. Set: ISBN 0–471–93453–4. Preis:£ 385.–," *Cryst. Res. Technol.*, vol. 30, no. 7, p. 920, 1995.

[35] M. S. Daw and M. I. Baskes, "Embedded-atom method: Derivation and application to impurities, surfaces, and other defects in metals," *Phys. Rev. B*, vol. 29, no. 12, p. 6443, 1984.

[36] M. W. Finnis and J. E. Sinclair, "A simple empirical N-body potential for transition metals," *Philos. Mag. A*, vol. 50, no. 1, pp. 45–55, 1984.

[37] M. I. Baskes, "Application of the embedded-atom method to covalent materials: a semiempirical potential for silicon," *Phys. Rev. Lett.*, vol. 59, no. 23, p. 2666, 1987.

[38] M. I. Pascuet and J. R. Fernández, "Atomic interaction of the MEAM type for the study of intermetallics in the Al–U alloy," *J. Nucl. Mater.*, vol. 467, pp. 229–239, 2015.

[39] Y.-M. Kim and B.-J. Lee, “Modified embedded-atom method interatomic potentials for the Ti–C and Ti–N binary systems,” *Acta Mater.*, vol. 56, no. 14, pp. 3481–3489, 2008.

[40] P. Brommer, A. Kiselev, D. Schopf, P. Beck, J. Roth, and H. R. Trebin, “Classical interaction potentials for diverse materials from ab initio data: A review of potfit,” *Model. Simul. Mater. Sci. Eng.*, 2015.

[41] A. I. Duff, M. W. Finnis, P. Maugis, B. J. Thijsse, and M. H. F. Sluiter, “MEAMfit: A reference-free modified embedded atom method (RF-MEAM) energy and force-fitting code,” *Comput. Phys. Commun.*, vol. 196, pp. 439–445, Nov. 2015.

[42] R. A. Johnson and D. J. Oh, “Analytic embedded atom method model for bcc metals,” *J. Mater. Res.*, vol. 4, no. 5, pp. 1195–1201, 1989.

[43] J. F. Ziegler, M. D. Ziegler, and J. P. Biersack, “SRIM–The stopping and range of ions in matter (2010),” *Nucl. Instruments Methods Phys. Res. Sect. B Beam Interact. with Mater. Atoms*, vol. 268, no. 11–12, pp. 1818–1823, 2010.

[44] “Crystallography Open Database.” .

[45] A. Stukowski, “Visualization and analysis of atomistic simulation data with OVITO–the Open Visualization Tool,” *Model. Simul. Mater. Sci. Eng.*, vol. 18, no. 1, p. 15012, 2009.

[46] A. Jain *et al.*, “Commentary: The Materials Project: A materials genome approach to accelerating materials innovation,” *Apl Mater.*, vol. 1, no. 1, p. 11002, 2013.

[47] B. Grabowski *et al.*, “Ab initio vibrational free energies including anharmonicity for multicomponent alloys,” *NPJ Comput. Mater.*, vol. 5, pp. 1–6, 2019.

[48] A. I. Duff *et al.*, “Improved method of calculating ab initio high-temperature thermodynamic properties with application to ZrC,” *Phys. Rev. B*, vol. 91, no. 21, p. 214311, 2015.

[49] “Recommended PAW Potential.” [Online]. Available: https://cms.mpi.univie.ac.at/vasp/vasp/Recommended_PAW_potentials_DFT_calculations_using_vasp_5_2.html.

[50] W. Humphrey, A. Dalke, and K. Schulten, “VMD: Visual molecular dynamics,” *J. Mol. Graph.*, vol. 14, no. 1, pp. 33–38, 1996.

[51] J. F. Nye, *Physical properties of crystals: their representation by tensors and matrices*. Oxford university press, 1985.

[52] Y. Mishin, M. J. Mehl, and D. A. Papaconstantopoulos, “Embedded-atom potential for B 2− NiAl,” *Phys. Rev. B*, vol. 65, no. 22, p. 224114, 2002.

[53] G. P. Purja Pun and Y. Mishin, “Development of an interatomic potential for the Ni-Al system,” *Philos. Mag.*, vol. 89, no. 34–36, pp. 3245–3267, 2009.

[54] F. X. Kayser and C. Stassis, “The elastic constants of Ni3Al at 0 and 23.5 C,” *Phys. status solidi*, vol. 64, no. 1, pp. 335–342, 1981.

[55] D. Kim, S.-L. Shang, and Z.-K. Liu, “Effects of alloying elements on elastic properties of Ni by first-principles calculations,” *Comput. Mater. Sci.*, vol. 47, no. 1, pp. 254–260, 2009.

APPENDIX

INCAR file.

Ground state Calculation.

ALGO = Normal

#IWAVPR = 11

EDIFF = 1e-06

ENCUT = 520

IBRION = 2

#ICHARG = 1

ISIF = 3

ISMEAR = 1

ISPIN = 2

SYM = 0

LORBIT = 11

LREAL = Auto

NPT Calculation:

SYSTEM = NiAl

PREC = Accurate

EDIFF= 5E-6

ENCUT = 520 # ENMAX in POTCAR

NELM = 40 # max number of selfconsistance steps, 40 normally

NELMIN = 4 # min number of SC steps

NSW = 5000 # max number of steps for IOM, # of MD steps

NBLOCK = 1 ; KBLOCK = 1000 # default =1

IBRION = 0 # -1 if NSW=1,0 ,0 for MD, 1 for newton, 2 for conj-grad

POTIM = 2.00 #

ISIF = 3 # 3=full vol relax, 2=no vol or shape change

ISMEAR = 1 # default

SIGMA = 0.2 # default Check this one!

LPLANE = .TRUE. # good for large cells

LREAL = .TRUE. # projection in reciprocal space, good for large cells

NPAR = 8 #

RWIGS = 1 1 1 # wigner seitz radius (need a number for each atom type)

VOSKOWN = 0 # default=0, 1 different interpolation formula

ALGO = Fast #

MAXMIX = 30 #something to do with dielectric function, also for MD

ISYM = 0 #switch of symmetry, for MD

SMASS = 0 #

LSCALAPACK = .TRUE.

LWAVE = .FALSE. # determines if WAVECAR is written

LCHARG = .TRUE. # determines if CHGCAR/CHG are written

LAECHG = .TRUE. # core to AECCAR0 and val to AECCAR2

NPT - related

MDALGO=3 # Langevin dynamics

TEBEG=1500

TEEND=1500

LANGEVIN_GAMMA = 10.0 10.0 10.0 # friction coef. for atomic DoFs

LANGEVIN_GAMMA_L=10.0 # friction coef. for lattice DoFs

PMASS=10 # mass for lattice DoFs

PSTRESS =.0001 # 0.001 0.001 0 0 0 Targeted stress tensor values in Kbar

NVT Calculation:

SYSTEM = Ni3Al

PREC = Accurate

ENCUT = 520   # ENMAX in POTCAR

NELM = 40   # max number of selfconsistance steps, 40 normally

NELMIN = 10   # min number of SC steps

EDIFF = 1.0e-6   # allowed error in total E

NSW = 5000   # max number of steps for IOM, # of MD steps

NBLOCK = 1 ; KBLOCK = 1000   # default =1

IBRION = 0   # -1 if NSW=1,0 ,0 for MD, 1 for newton, 2 for conj-grad

POTIM = 1.00   #

ISIF = 2   # 3=full vol relax, 2=no vol or shape change

ISMEAR = -5

SIGMA = 0.05   # default Check this one!

LPLANE = .TRUE.   # good for large cells

LREAL = .TRUE.   # projection in reciprocal space, good for large cells

NPAR = 4   #

RWIGS = 1 1 1   # wigner seitz radius (need a number for each atom type)

VOSKOWN = 0 # default=0, 1 different interpolation formula

ALGO = Fast #

LWAVE = .FALSE. # determines if WAVECAR is written

LCHARG = .FALSE. # determines if CHGCAR/CHG are written

MAXMIX = 30 #something to do with dielectric function, also for MD

ISYM = 0 #switch of symmetry, for MD

SMASS = 0 #

TEBEG = 2000 #temperature for MD

TEEND = 2000

CIJ Calculation:

ALGO = Fast

#IWAVPR = 11

EDIFF = 5e-06

ENCUT = 520

IBRION = 6

#ICHARG = 1

ISIF = 3

ISMEAR = 0

ISPIN = 2

ISYM = 0

LORBIT = 11

LREAL = Auto

LWAVE = False

#MAGMOM = 202*0.6

#NELECT = 288.0

NELM = 100

NPAR = 4

NSW = 1000

PREC = Accurate

SIGMA = 0.05

LAMMPS

Thermal Stability.

```
units          metal
boundary       p p p
atom_style     atomic


# ---------- Create Atoms ----------------------
read_data data.AlNi
mass           1  27
mass           2  58.6934
# ---------- Calling the potential file----------------------
pair_style     eam/alloy
pair_coeff     * * AlNi.eam.alloy_1 Al Ni
```

```
# ---------- Running NPT simulation----------------

timestep        0.001

velocity all create 300 12345 mom yes rot no

dump            dump all atom 10 dump_iso_1500K_model_5.dat

#restart        1000 restart.*

thermo          10

thermo_style    custom step temp etotal pe press vol lx ly lz pxx pyy pzz pyz pxz pxy

fix 1 all npt temp 300 300 1 iso 0 0 1

run             10000

unfix           1
```